



Leibniz-Institut für
Festkörper- und
Werkstoffforschung
Dresden



Workshop Weil Fermions in Condensed Matter
IIP, Natal, Brazil, July 1 to August 27, 2019

**Topology- and geometry-driven properties
of advanced micro- and nanoarchitectures:
Introduction into topological matter and its possible
geometric designs**

Vladimir Fomin

*Institute for Integrative Nanosciences (IIN),
Leibniz Institute for Solid State and Materials Research (IFW) Dresden,
D-01069 Dresden, Germany*

OUTLINE

Part I

1. Topologic effects in quantum rings by virtue of double connectivity.
Novel GaAs/AlAs core-multishell nanowires and optical Aharonov–Bohm oscillations in GaAs/AlAs crystal-phase quantum rings
2. Topologic effects in Möbius rings

Part II

3. Topologic states of light in microcavities
4. Phononic multishell metamaterials

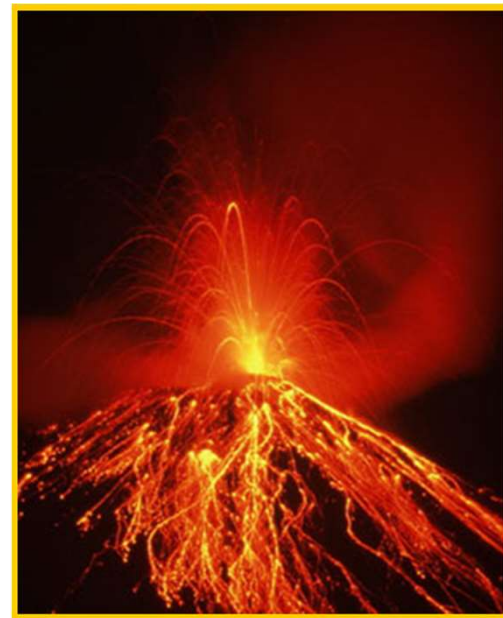
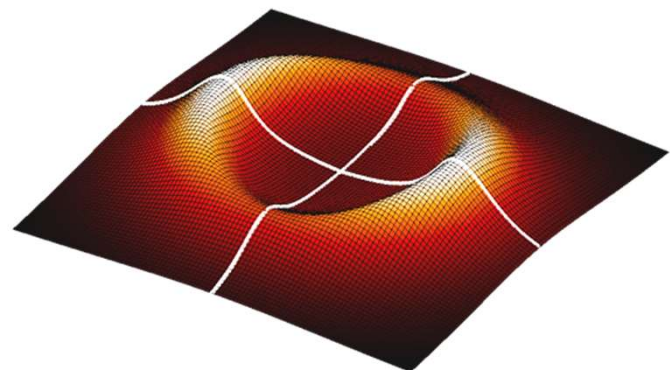
Part III

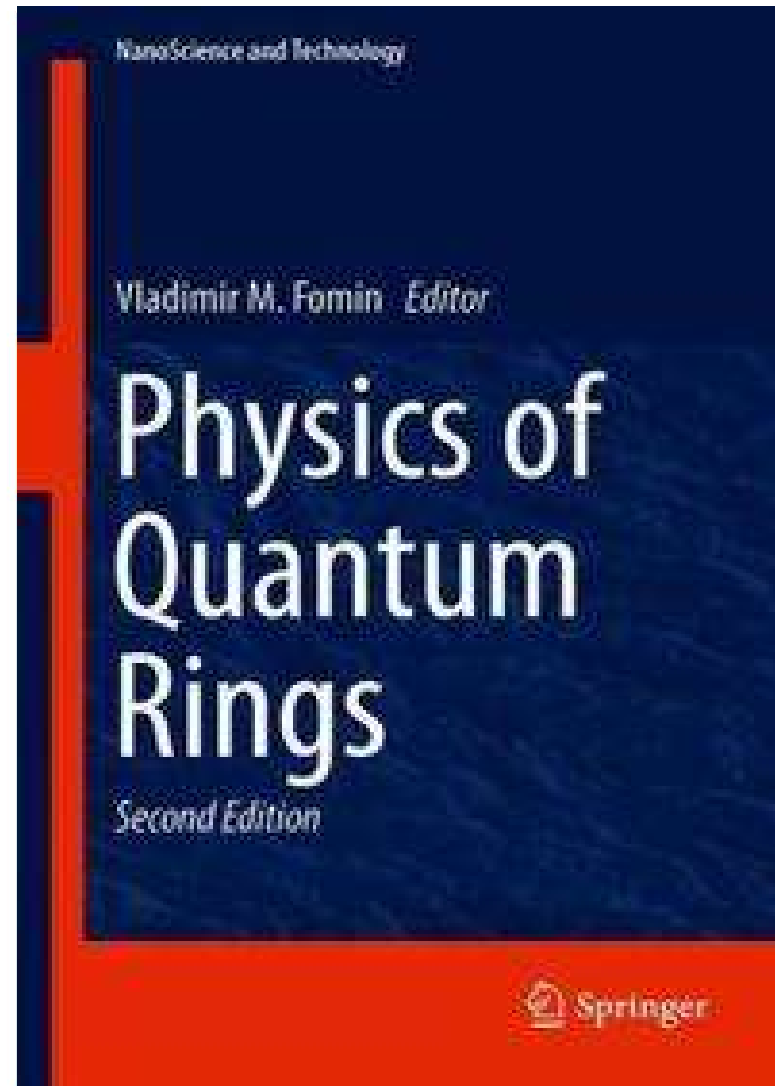
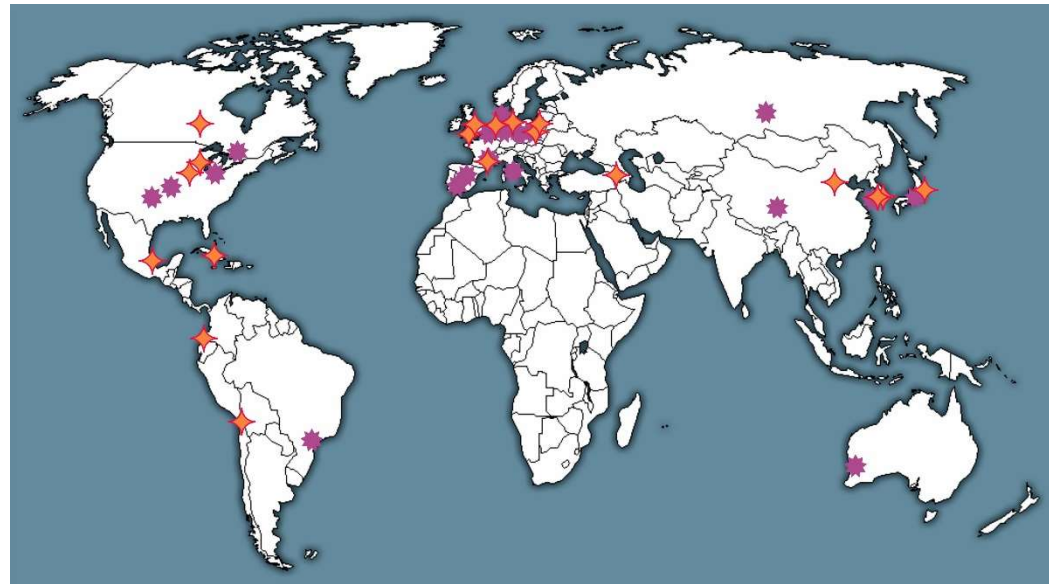
5. Geometry-driven effects in superconductor nanoarchitectures

V. M. Fomin, in: Functional Nanostructures and Metamaterials for Superconducting Spintronics, A. Sidorenko (Ed.), Springer International Publishing, Cham, 2018, pp. 195-220.

V. M. Fomin, Topology and geometry controlled properties of nanoarchitectures, Phys. Stat. Sol. – Rapid Research Letters 13, 1800595 (2019).

1. TOPOLOGIC EFFECTS IN QUANTUM RINGS BY VIRTUE OF DOUBLE CONNECTIVITY





**V. M. Fomin (Ed.), Physics of Quantum Rings, Series: NanoSci. Technol.
Springer, Berlin, Heidelberg a. o., 2014, ISBN 978-3-642-39196-5, 487pp.**

Second edition, Springer International, 2018, 586 pp.

Geometric phase (Pancharatnam-Berry phase)

$$i\hbar|\dot{\psi}(t)\rangle = H(\mathbf{R}(t))|\psi(t)\rangle \quad \mathbf{R} \equiv \mathbf{R}(t) \text{ a closed path} \quad \mathbf{R}(0) = \mathbf{R}(T)$$

$$H(\mathbf{R})|n(\mathbf{R})\rangle = E_n(\mathbf{R})|n(\mathbf{R})\rangle \text{ at any instant t}$$

adiabatic approximation $|n(\mathbf{R}(0))\rangle$ evolves into $|n(\mathbf{R}(t))\rangle$

$$|\psi(t)\rangle = \exp\left[-\frac{i}{\hbar} \int_0^t d\tau E_n(\mathbf{R}(\tau))\right] \exp[i\gamma_n(t)] |n(\mathbf{R}(t))\rangle$$

Equation for the geometric phase: $\dot{\gamma}_n(t) = i\langle n(\mathbf{R}(t))|\nabla_{\mathbf{R}}n(\mathbf{R}(t))\rangle \cdot \dot{\mathbf{R}}(t)$

$$|\psi(T)\rangle = \exp\left[-\frac{i}{\hbar} \int_0^T d\tau E_n(\mathbf{R}(\tau))\right] \exp[i\gamma_n(C)] |\psi(0)\rangle$$

Change of the geometric phase over the closed path C:

$$\gamma_n(C) = i \oint_C \langle n(\mathbf{R})|\nabla_{\mathbf{R}}n(\mathbf{R})\rangle \cdot d\mathbf{R} \quad \text{Berry connection}$$

S. Pancharatnam, Proc. Indian Acad. Sci. A 44, 247 (1956).

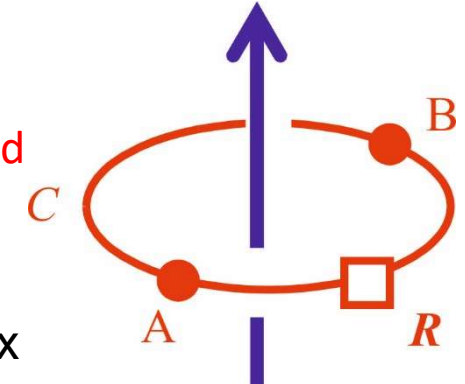
M.V. Berry, Proc. R. Soc. Lond. A 392, 45 (1984).

Geometric phase due to the doubly-connectedness

A magnetic flux line carrying the flux Φ

The paths $C(2\pi)$ around the flux line are unshrinkable

A particle with charge q confined to a box at \mathbf{R} outside of the flux



$H(\mathbf{p}, \mathbf{r} - \mathbf{R})$: eigenfunctions $\psi_n(\mathbf{r} - \mathbf{R})$ and eigenenergies E_n

$$H(\mathbf{p} - q\mathbf{A}(\mathbf{r}), \mathbf{r} - \mathbf{R}) |n(\mathbf{R})\rangle = E_n |n(\mathbf{R})\rangle$$

Magnetic phase factor: $\langle \mathbf{r} | n(\mathbf{R}) \rangle = \exp \left[i \frac{q}{\hbar} \int_{\mathbf{R}}^{\mathbf{r}} d\boldsymbol{\rho} \cdot \mathbf{A}(\boldsymbol{\rho}) \right] \psi_n(\mathbf{r} - \mathbf{R})$

$$\langle n(\mathbf{R}) | \nabla_{\mathbf{R}} n(\mathbf{R}) \rangle = \int d^3 r \psi_n^*(\mathbf{r} - \mathbf{R}) \left[-i \frac{q}{\hbar} \mathbf{A}(\mathbf{R}) \psi(\mathbf{r} - \mathbf{R}) + \nabla_{\mathbf{R}} \psi_n(\mathbf{r} - \mathbf{R}) \right] = -i \frac{q}{\hbar} \mathbf{A}(\mathbf{R})$$

$$\gamma_n(C) = \frac{q}{\hbar} \oint_C \mathbf{A}(\mathbf{R}) \cdot d\mathbf{R} = \frac{q\Phi}{\hbar}$$

$$|\psi(\Phi)\rangle = \exp \left[i \frac{2\pi\Phi}{\Phi_0} \right] |\psi(\Phi=0)\rangle$$

$$\frac{q}{\hbar} = \frac{2\pi}{\Phi_0}, \Phi_0 = \frac{\hbar}{q}.$$

A charged particle gains the phase as it moves over C .

Confinement to a doubly connected nanostructure: Aharonov-Bohm effect in a quantum ring

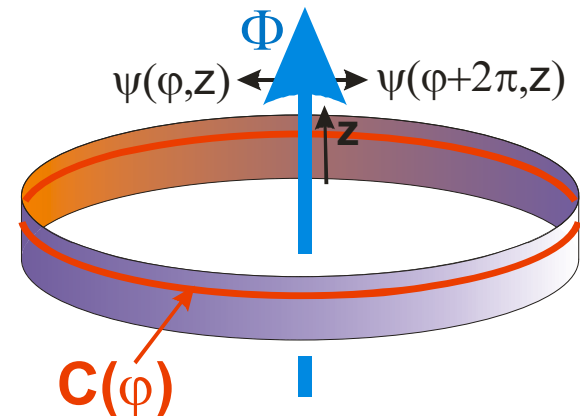
ϕ and \mathbf{A} give a complete description, they are not physically observable

gauge transformation: $\phi \rightarrow \phi' = \phi - \frac{\partial \Lambda}{\partial t}; \mathbf{A} \rightarrow \mathbf{A}' = \mathbf{A} + \nabla \Lambda; \psi \rightarrow \psi' = \exp\left(-i\frac{e}{\hbar}\Lambda\right)\psi$

$$\Lambda = - \int_C \mathbf{A} d\mathbf{l} \Rightarrow \mathbf{A}' = 0 \quad \psi'(\varphi, z) = \exp\left(i\frac{e}{\hbar} \int_{C(\varphi)} \mathbf{A} d\mathbf{l}\right) \psi(\varphi, z)$$

$$\psi'(\varphi + 2\pi, z) = \exp\left(i2\pi \frac{\Phi}{\Phi_0}\right) \exp\left(i\frac{e}{\hbar} \int_{C(\varphi)} \mathbf{A} d\mathbf{l}\right) \psi(\varphi + 2\pi, z)$$

$$\int_{C(2\pi)} \mathbf{A} d\mathbf{l} = \Phi; \quad \Phi_0 = h/e$$



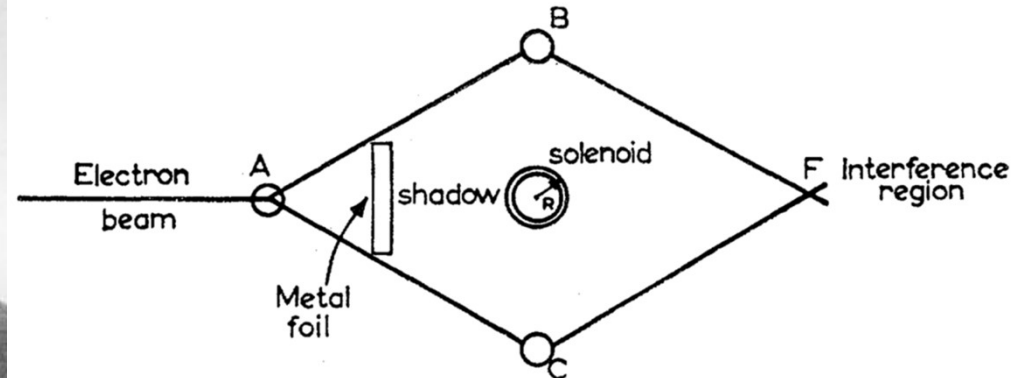
Single-valuedness: $\psi(\varphi + 2\pi, z) = \exp(i2\pi m) \psi(\varphi, z); m = 0, \pm 1, \pm 2, \dots$

Flux-modified boundary condition:

$$\psi'(\varphi + 2\pi, z) = \boxed{\exp\left(i2\pi \frac{\Phi}{\Phi_0}\right)} \psi'(\varphi, z)$$

Ehrenberg-Siday-Aharonov-Bohm effect

The periodic phase factor becomes observable through interference effects!

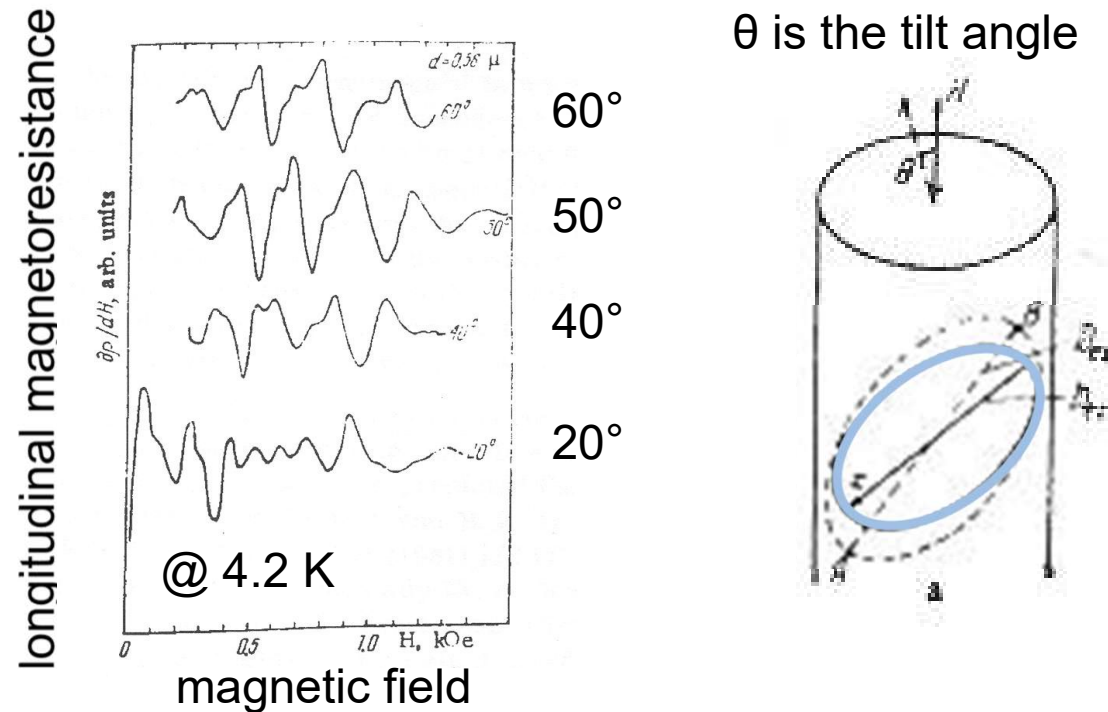


domain. We shall show that, contrary to the conclusions of classical mechanics, there exist effects of potentials on charged particles, even in the region where all the fields (and therefore the forces on the particles) vanish. We shall then discuss possible experiments to test these conclusions; and, finally, we shall suggest

W. Ehrenberg and R. E. Siday, Proc. Phys. Soc., Ser. B 62, 8 (1949).

Y. Aharonov and D. Bohm, Phys. Rev. 115, 485 (1959).

Quantum interference effect for flux quantization in nonsuperconducting condensed matter



In bismuth single-crystal whiskers 200–800 nm thick, oscillations in the longitudinal magnetoresistance with the period $\Phi_0/\cos\theta$ are a manifestation of the Aharonov-Bohm effect.

[1] N.B.Brandt, D.V.Gitsu, A.A.Nikolaeva, Ya.G.Ponomarev , JETP Lett. 24, 272 (1976)

[2] N.B.Brandt, E.N.Bogachev, D.V.Gitsu, G.A.Gogadze, I.O.Kulik, A.A.Nikolaeva,
Ya.G.Ponomarev, Sov. J. Low Temp. Phys. 8, 358 (1982)

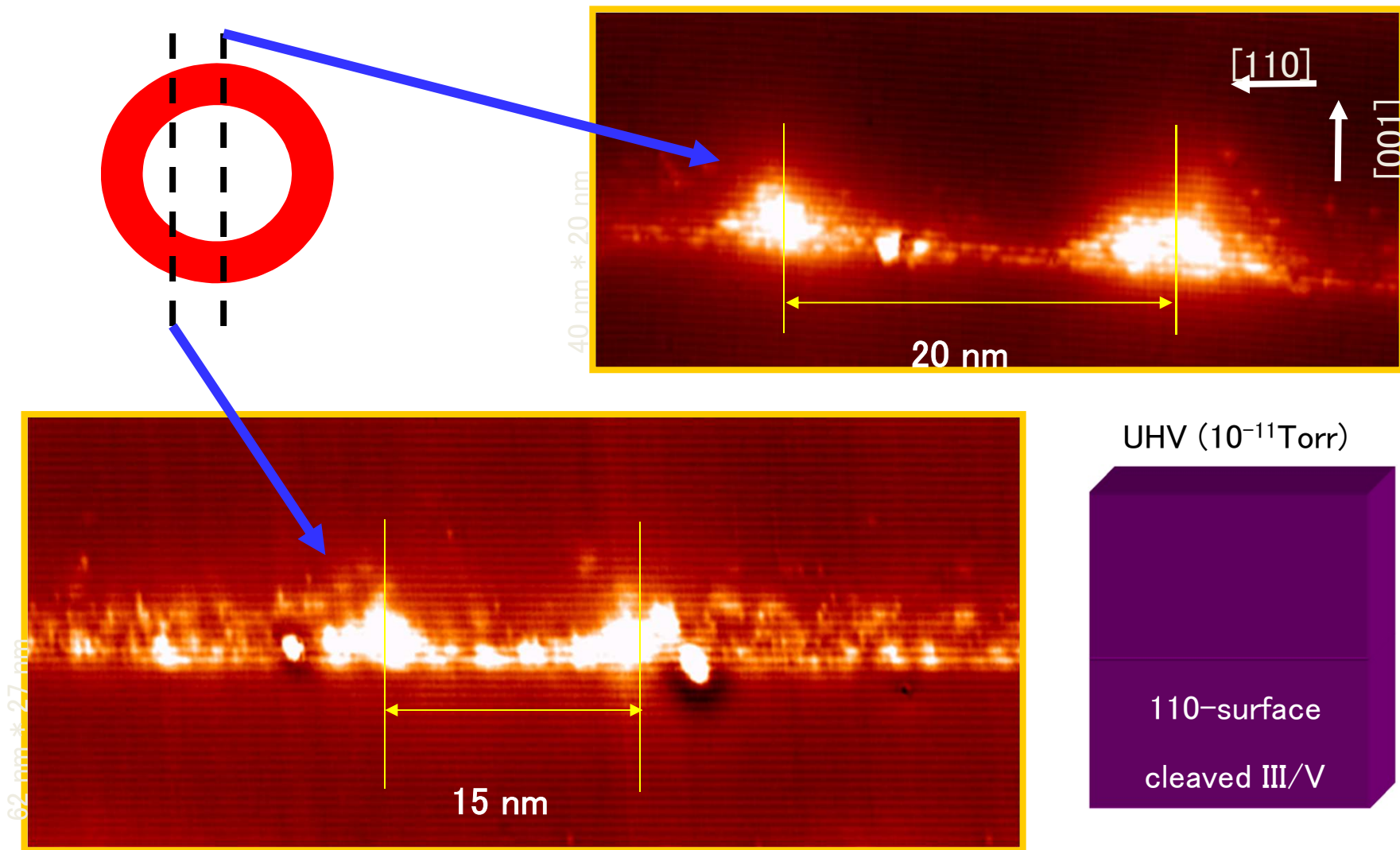
Self-assembled quantum rings



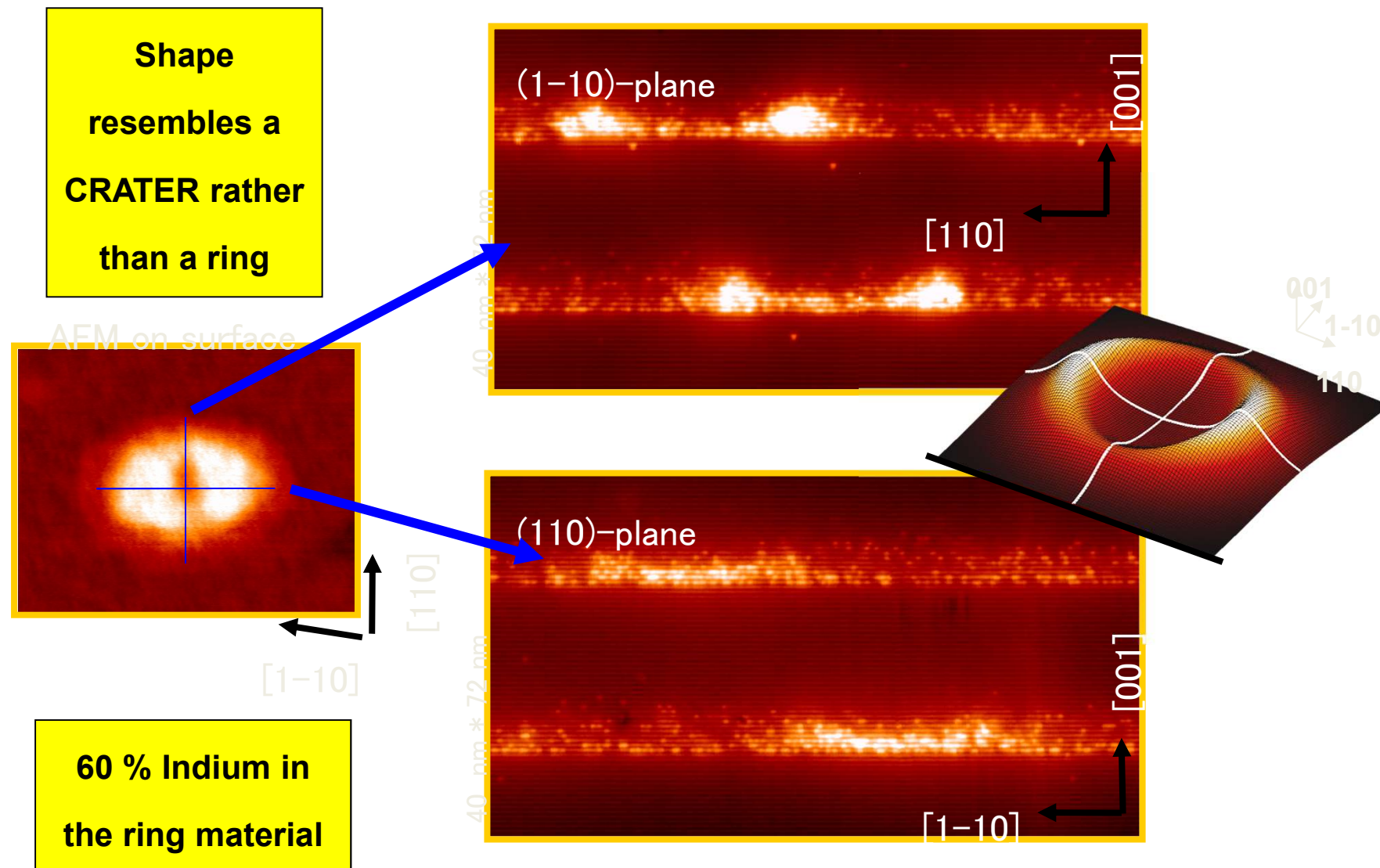
- 1) InAs quantum dot formation by Stranski-Krastanov growth (1.9 ML at 540 °C 0.2 ML/s)
- 2) Capping with 2 nm GaAs at 500 °C
- 3) Annealing for 60 s at 500 °C under As₂ flux

J. M. Garcia, G. Medeiros-Ribeiro, K. Schmidt, T. Ngo, J. L. Feng, A. Lorke, J. Kotthaus, and P. M. Petroff, Appl. Phys. Lett. 71, 2014 (1997).

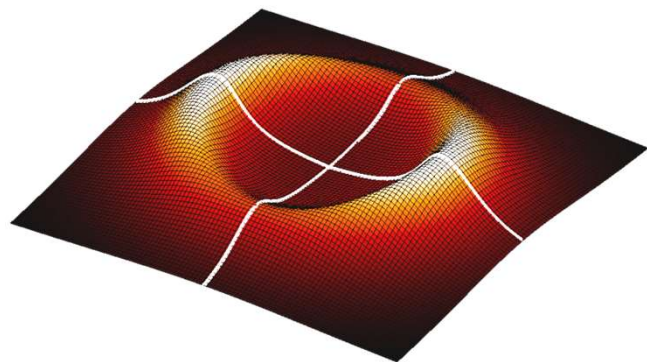
Self-assembled quantum rings: XSTM characterization



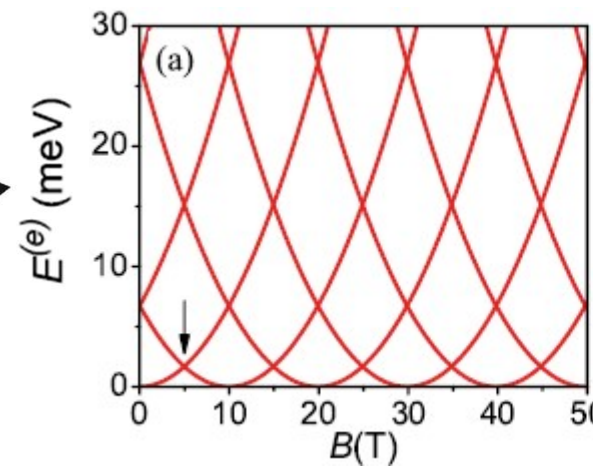
P. Offermans et al., Appl. Phys. Lett. 87, 131902 (2005).



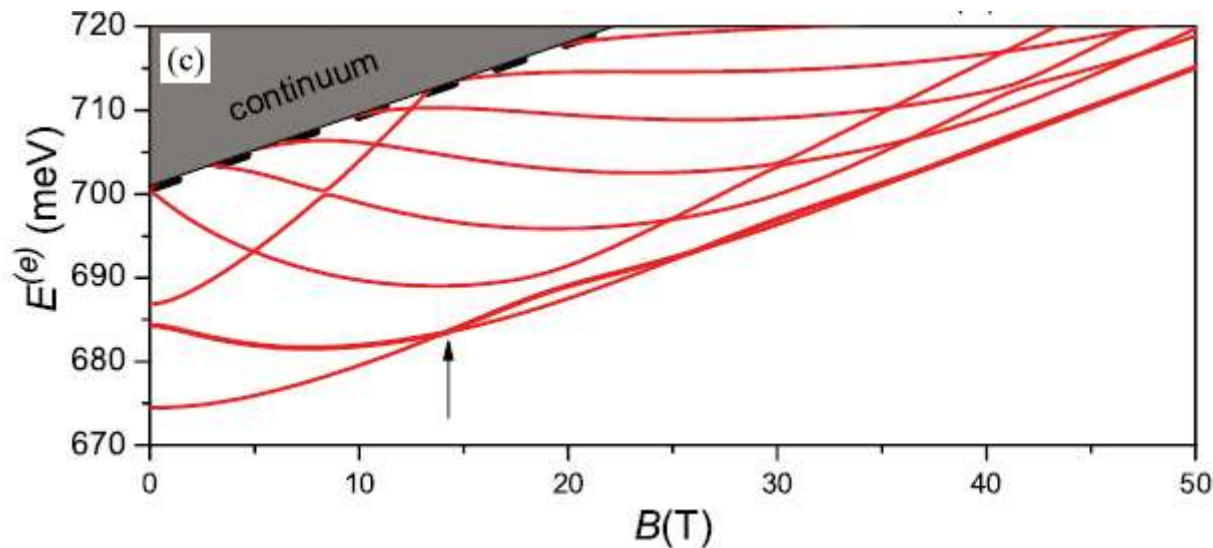
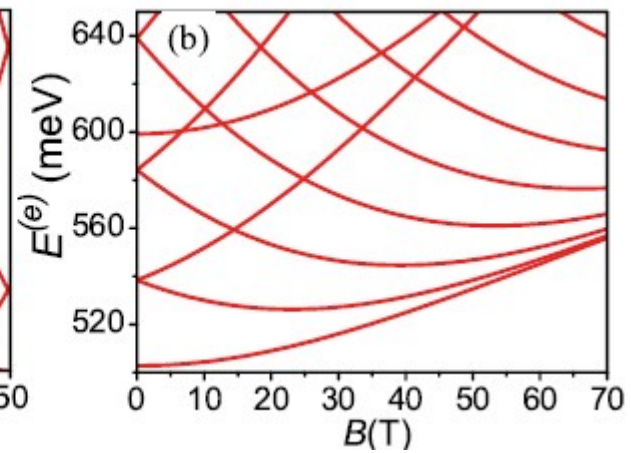
P. Offermans, P. M. Koenraad, J. H. Wolter, J. M. García, and D. Granados, V. M. Fomin, V. N. Gladilin, and J. T. Devreese, Appl. Phys. Lett. 87, 131902 (2005).



ideal ring



disk-shaped quantum dot



self-assembled ring-like nanostructure

V. M. Fomin et al., Phys. Rev. B 76, 235320 (2007).

Electrons and holes in quantum rings: Adiabatic approach

$$H_\beta \Psi^{(\beta)}(\mathbf{r}) = E \Psi^{(\beta)}(\mathbf{r}) \quad \beta = e, h$$

Adiabatic Ansatz

$$\Psi^{(\beta)}(\mathbf{r}) = \psi_k^{(\beta)}(z; \rho, \varphi) \Phi_{kj}^{(\beta)}(\rho, \varphi),$$

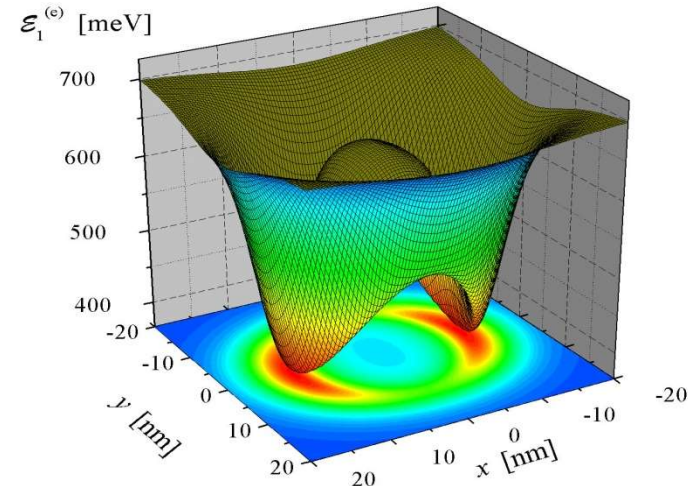
“Fast” degree of freedom:

$$\left[-\frac{\hbar^2}{2} \frac{\partial}{\partial z} \frac{1}{m_\beta(\rho, \varphi, z)} \frac{\partial}{\partial z} \pm V_\beta(\rho, \varphi, z) \pm \delta E_\beta(\rho, \varphi, z) \mp eV_P(\rho, \varphi, z) \right] \psi_k^{(\beta)}(z; \rho, \varphi)$$

$$= \mathcal{E}_k^{(\beta)}(\rho, \varphi) \psi_k^{(\beta)}(z; \rho, \varphi).$$

“Slow” degree of freedom:

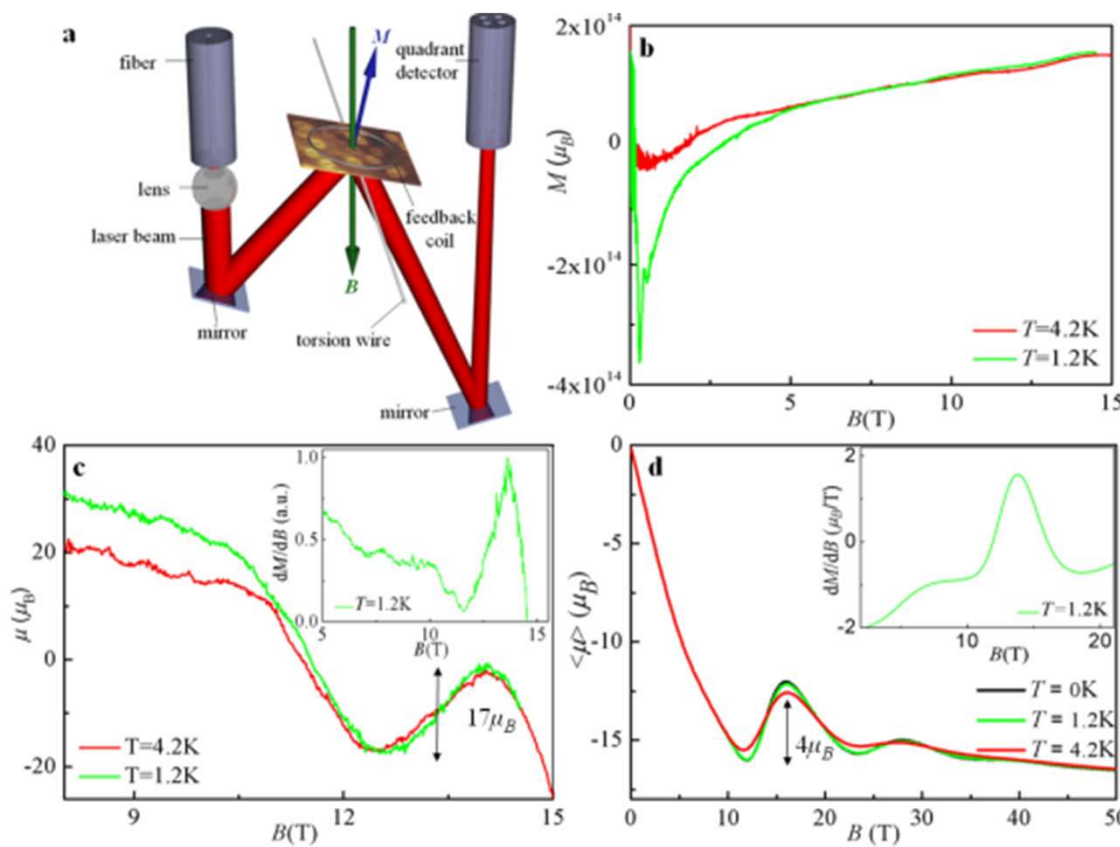
$$\left[-\frac{\hbar^2}{2} \left(\nabla_{\rho, \varphi} \mp \frac{e}{\hbar} \mathbf{A} \right) \frac{1}{m_k^{(\beta)}(\rho, \varphi)} \left(\nabla_{\rho, \varphi} \mp \frac{e}{\hbar} \mathbf{A} \right) + \mathcal{E}_k^{(\beta)}(\rho, \varphi) \right] \Phi_{kj}^{(\beta)}(\rho, \varphi) = E_{kj}^{(\beta)} \Phi_{kj}^{(\beta)}(\rho, \varphi),$$



V. M. Fomin, V. N. Gladilin, S. N. Klimin, J. T. Devreese, N. A. J. M. Kleemans, and P. M. Koenraad, Phys. Rev. B 76, 235320 (2007).

Quantum interference effects in the magnetisation

InGaAs/GaAs SAQRs @1.2K and 4.2K

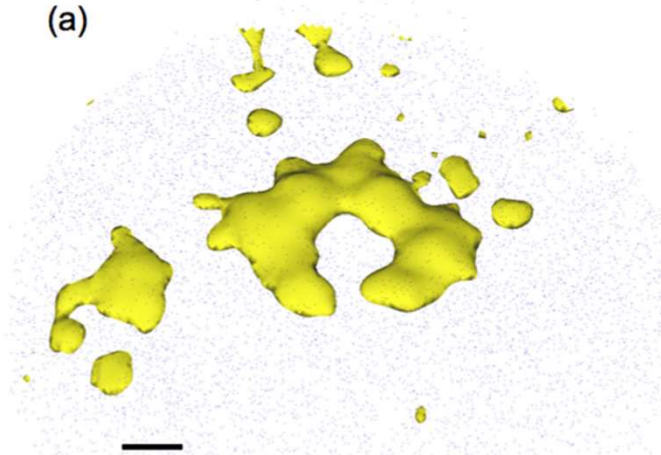


N. A. J. M. Kleemans, I. M. A. Bominaar-Silkens, V. M. Fomin, V. N. Gladilin, D. Granados, A. G. Taboada, J. M. García, P. Offermans, U. Zeitler, P. C. M. Christianen, J. C. Maan, J. T. Devreese, and P. M. Koenraad, Phys. Rev. Lett. 99, 146808 (2007).
V. M. Fomin, V. N. Gladilin, S. N. Klimin, J. T. Devreese, N. A. J. M. Kleemans, and P. M. Koenraad, Phys. Rev. B 76, 235320 (2007).

Diversification of materials

Disintergration of GaSb/GaAs QDs upon capping

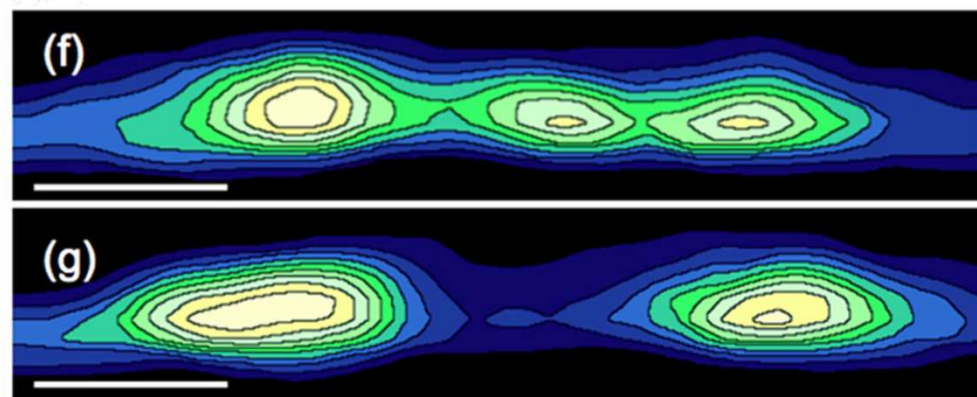
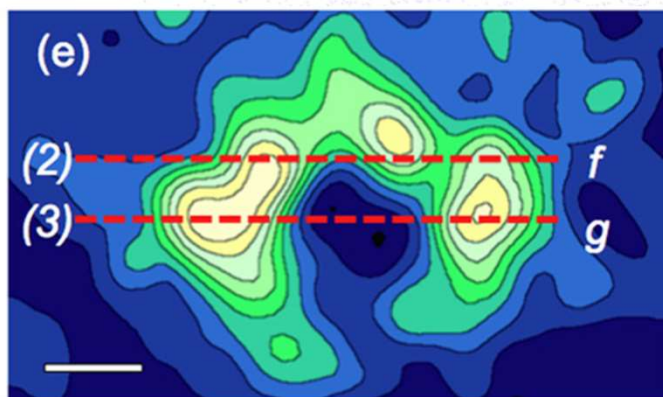
(a)



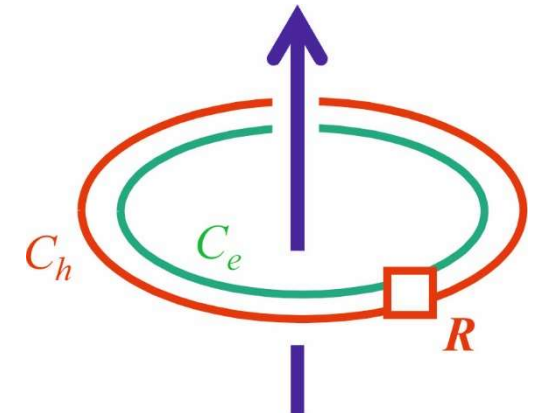
Atom Probe Tomography
has contributed to major
advances in materials science

9% Sb concentration

All scale bars are 5 nm



A. J. Martin, J. Hwang, E. A. Marquis, E. Smakman, T. W. Saucer, G. V. Rodriguez,
A. H. Hunter, V. Sih, P. M. Koenraad, J. D. Phillips, J. Millunchick, Appl. Phys. Lett.
102, 113103 (2013).



The wave function of the exciton

$$|\Psi(\Phi_h, \Phi_e)\rangle = \exp\left[i \frac{e(\Phi_h - \Phi_e)}{\hbar}\right] |\Psi(\Phi_h = 0, \Phi_e = 0)\rangle \quad (1.10)$$

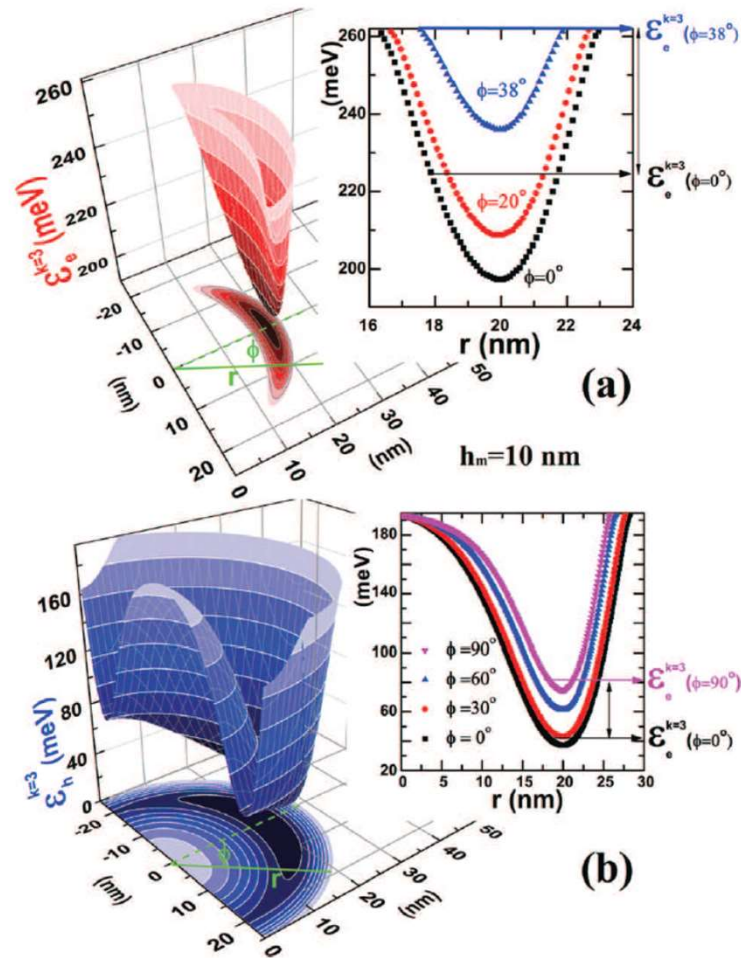
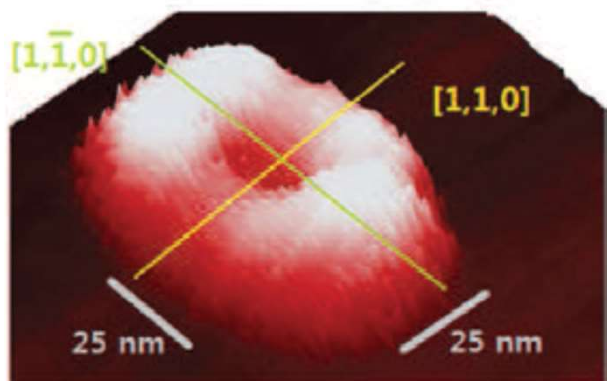
gains a phase, which is determined by a difference between the magnetic fluxes through the paths C_h and C_e encircled by the hole and the electron, respectively:

$$\Phi_h = \frac{e}{\hbar} \oint_{C_h} \mathbf{A}(\mathbf{R}) \cdot d\mathbf{R}, \quad \Phi_e = \frac{e}{\hbar} \oint_{C_e} \mathbf{A}(\mathbf{R}) \cdot d\mathbf{R}. \quad (1.11)$$

If the exciton is polarized, C_h and C_e are different from each other.

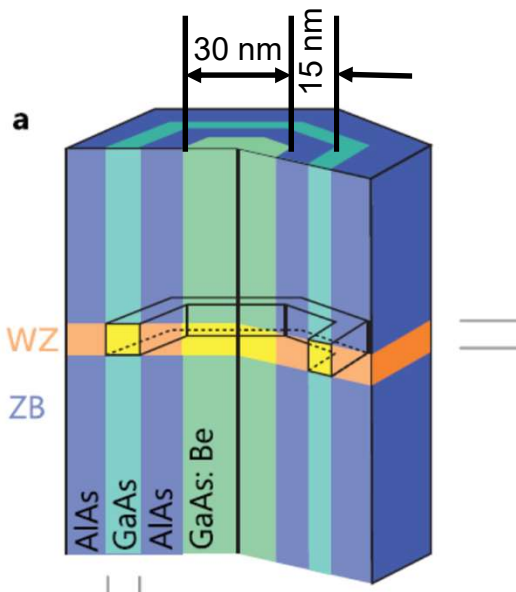
The quantum interference is caused by the magnetic flux $\Phi_h - \Phi_e$.

Asymmetry of localised states in a single GaAs quantum ring



H. D. Kim, K. Kyhm, R. A. Taylor, G. Nogues, K. C. Je, E. H. Lee, and J. D. Song, Appl. Phys. Lett. 102, 033112 (2013)

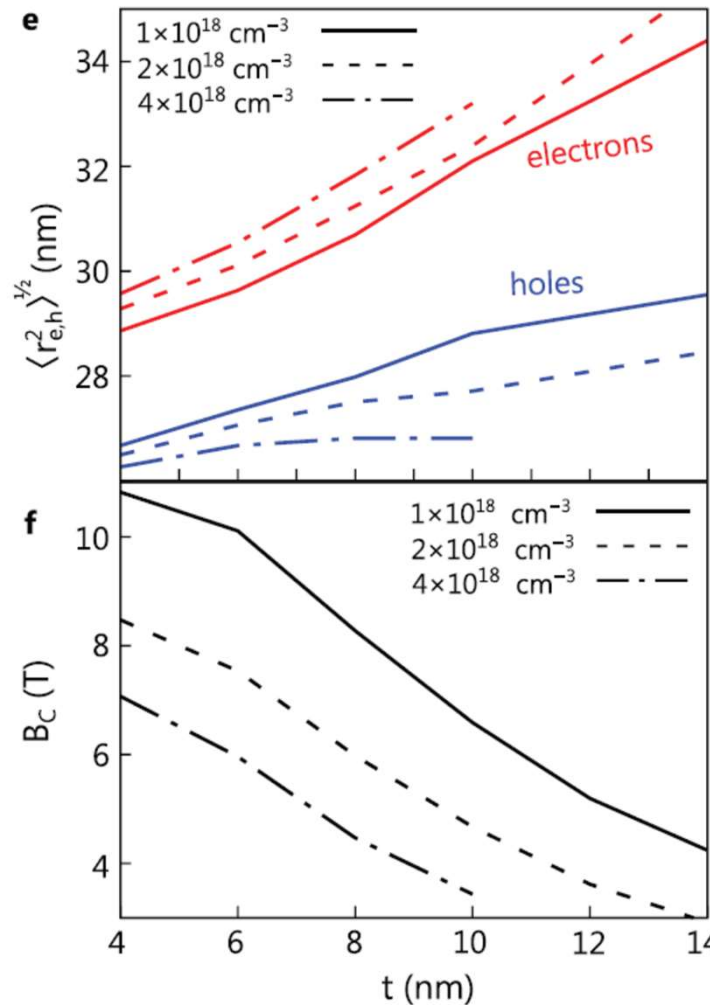
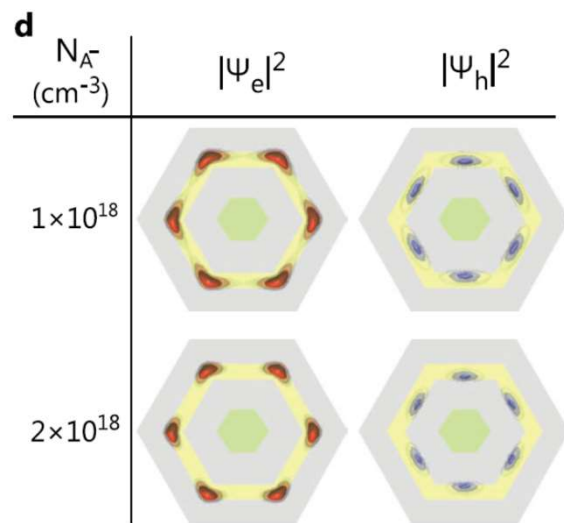
Novel GaAs/AlAs core-multishell nanowires



Schematic representation of the
GaAs/AlAs core-multishell nanowire.
A WZ segment created by a twin boundary
propagates through the entire diameter.

Radii of the electron and hole states and the characteristic magnetic field

Distribution of electron and hole charge density across the section of the QR for $t = 7 \text{ nm}$

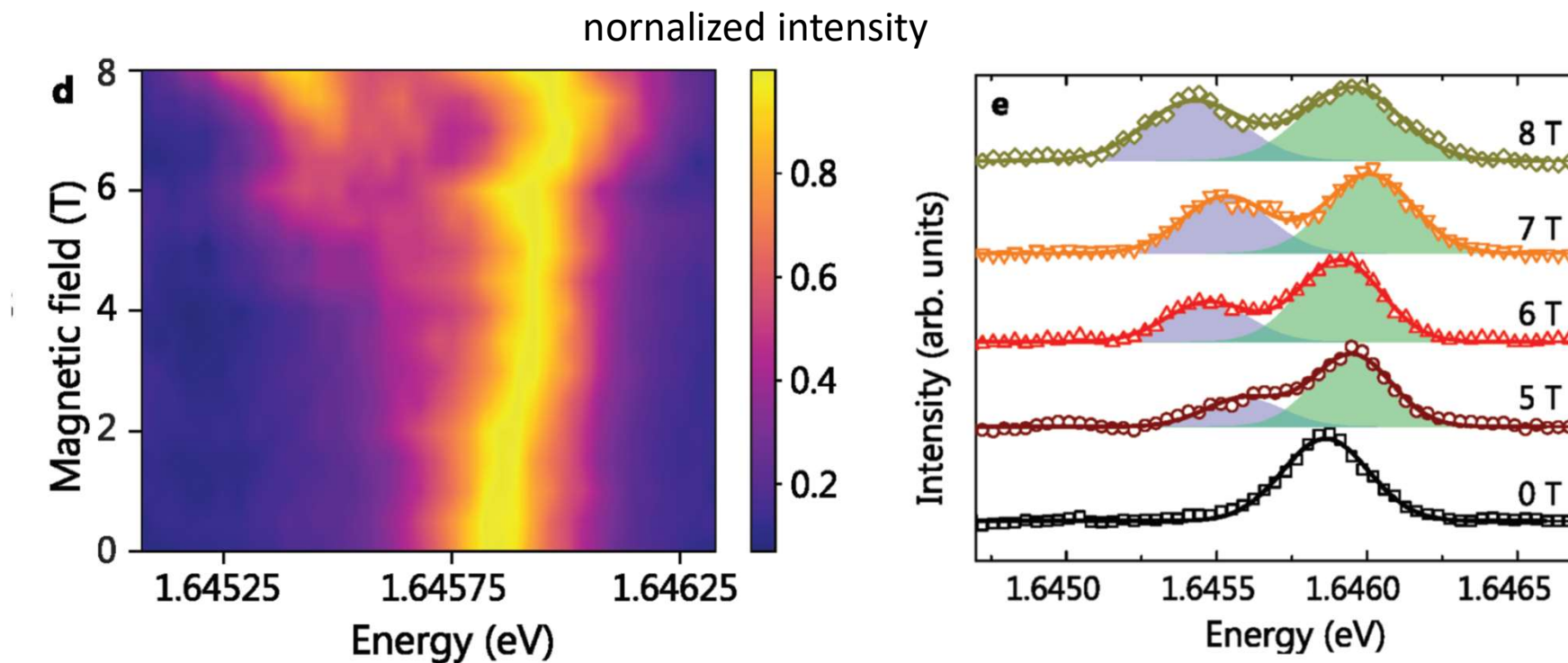


RMS radii of the electron and hole charge densities as a function of t for three different ionized acceptor concentrations.

Characteristic magnetic field that induces a 2π phase shift to the exciton wave function:

$$B_C = \frac{\Phi_0}{\pi |\langle r_e^2 \rangle - \langle r_h^2 \rangle|}$$

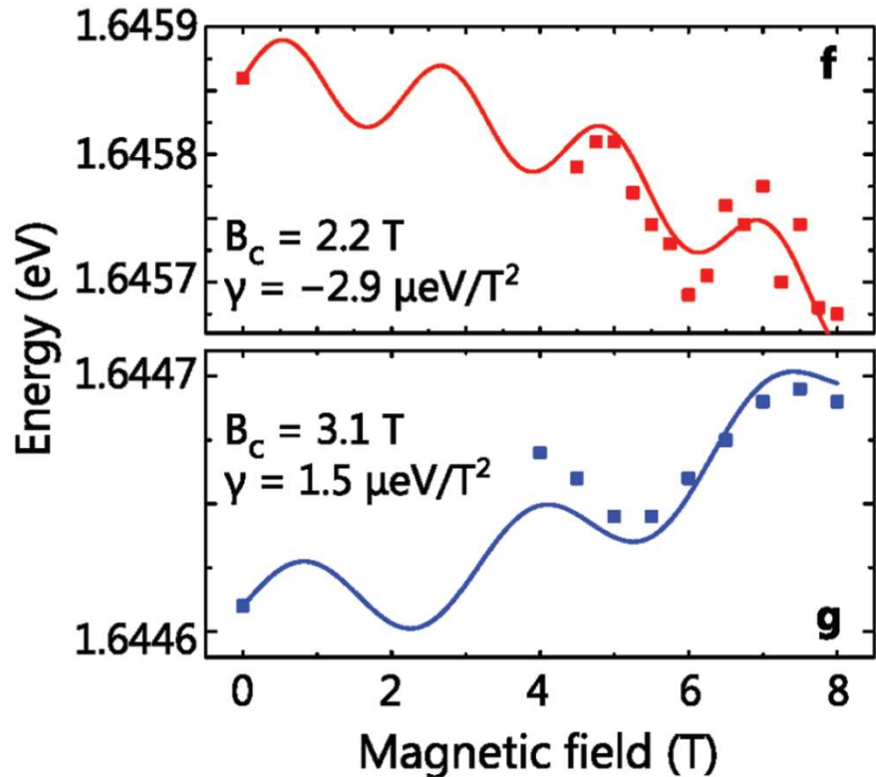
Optical Aharonov–Bohm oscillations in GaAs/AlAs crystal-phase quantum rings



Evolution of the exciton energy in a magnetic field for the QR in a nanowire. The magnetic field is parallel to the nanowire axis.
The spectra have been normalized.

PL spectra at selected magnetic fields (symbols). The lines are the results of Gaussian fits.
The blue and green shaded areas highlight the contribution of each Zeeman split state.

Optical Aharanov–Bohm oscillations in GaAs/AlAs crystal-phase quantum rings



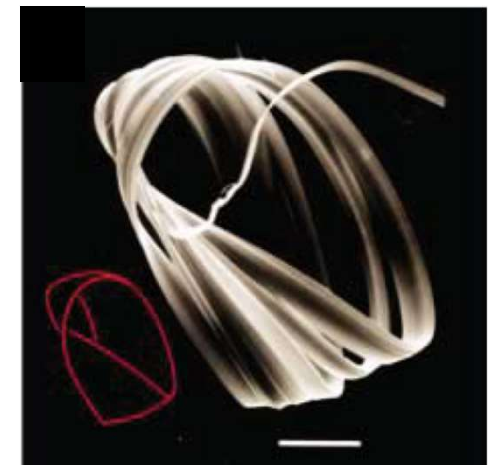
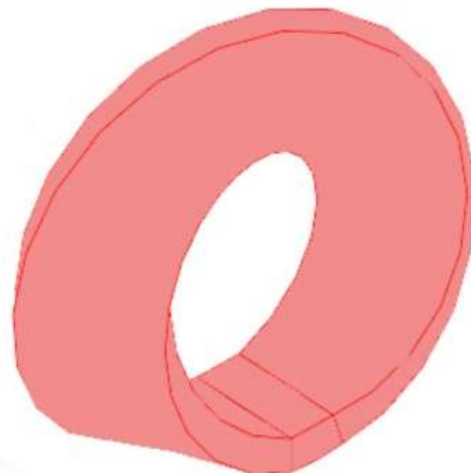
Dependence of the average energy of the Zeeman split states on magnetic field for two QRs.

Solid lines: fits accounting for AB oscillations and a diamagnetic shift.

2. TOPOLOGIC EFFECTS IN MÖBIUS RINGS



A. F. Möbius



Möbius strip

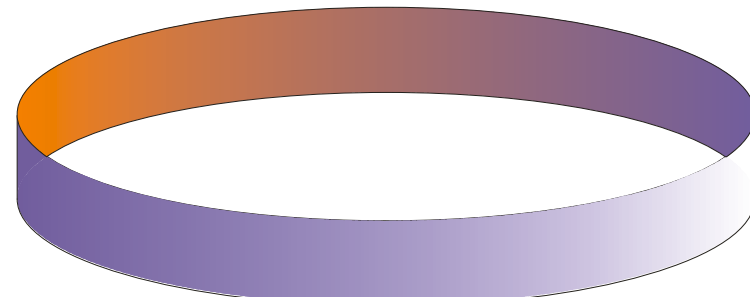
§. 11. Von der verschiedenartigen Form der zweierlei Zonenflächen kann man sich eine sehr anschauliche Vorstellung mittelst eines Papierstreifens verschaffen, welcher die Form eines Rechtecks hat. Sind A, B, B', A' (vergl. Fig. 1) die vier Ecken desselben in



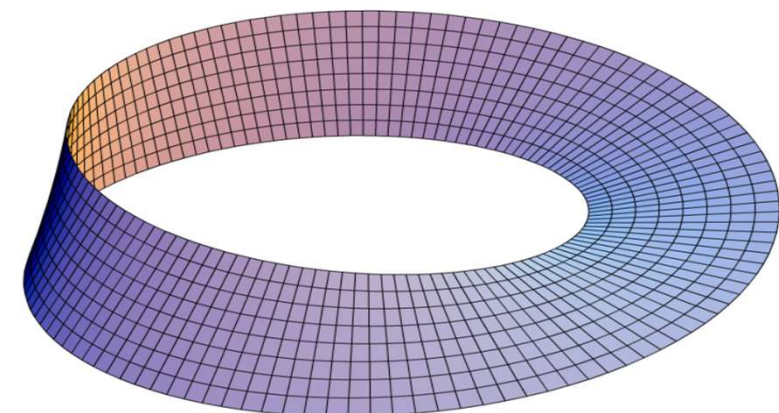
Fig. 1.

ihrer Aufeinanderfolge, und wird er hierauf gebogen, so dass die Kante $A'B'$ sich stets parallel bleibt, bis sie zuletzt mit AB zusammenfällt, so erhält der Streifen die Form einer Cylinderfläche, also einer zweiseitigen Zone, welche die

zwei nunmehr kreisförmigen Kanten AA' und BB' des anfänglichen Rechtecks zu ihren zwei Grenzlinien hat. — Man kann aber auch, dafern das eine Paar paralleler Kanten AA' und BB' gegen das andere AB und $A'B'$ hinreichend gross ist, A' mit B , und B' mit A zur Coïncidenz bringen, indem man zuvor, das eine Ende AB des Streifens festhaltend, das andere Ende $A'B'$ um die Längenaxe des



Bending \Rightarrow two-sided cylindric strip



The Möbius strip, a two dimensional surface with only one side, was discovered independently by Möbius and Johann Benedict Listing in 1858.

Affixing the ends of a rectangular strip after first having given one of the ends a one-half twist \Rightarrow one-sided surface

A. F. Möbius, Über die Bestimmung des Inhaltes eines Polyëders [On the determination of the volume of a polyhedron] (1865).

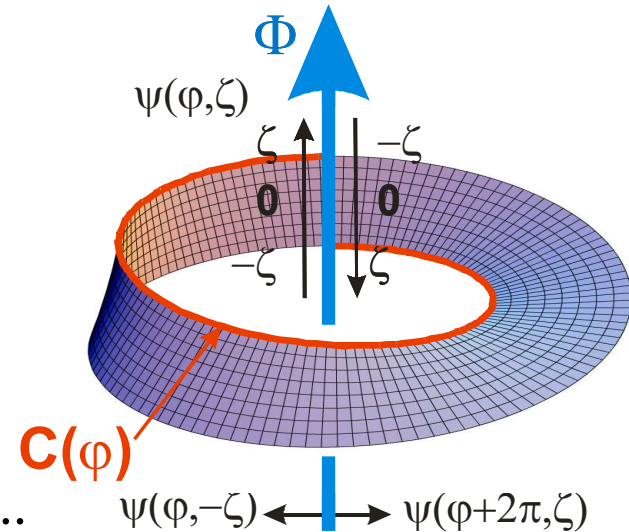
Aharonov-Bohm effect in a Möbius strip

$$\psi'(\varphi; \zeta) = \exp\left(i \frac{e}{\hbar} \int_{C(\varphi)} \mathbf{A} d\mathbf{l}\right) \psi(\varphi, \zeta)$$

$$\psi'(\varphi + 2\pi, \zeta) = \exp\left(i 2\pi \frac{\Phi}{\Phi_0}\right) \exp\left(i \frac{e}{\hbar} \int_{C(\varphi)} \mathbf{A} d\mathbf{l}\right) \psi(\varphi + 2\pi, \zeta)$$

Single-valuedness:

$$\psi(\varphi + 2\pi, \zeta) = \exp(i 2\pi m) \psi(\varphi, -\zeta); m = 0, \pm 1, \pm 2, \dots$$

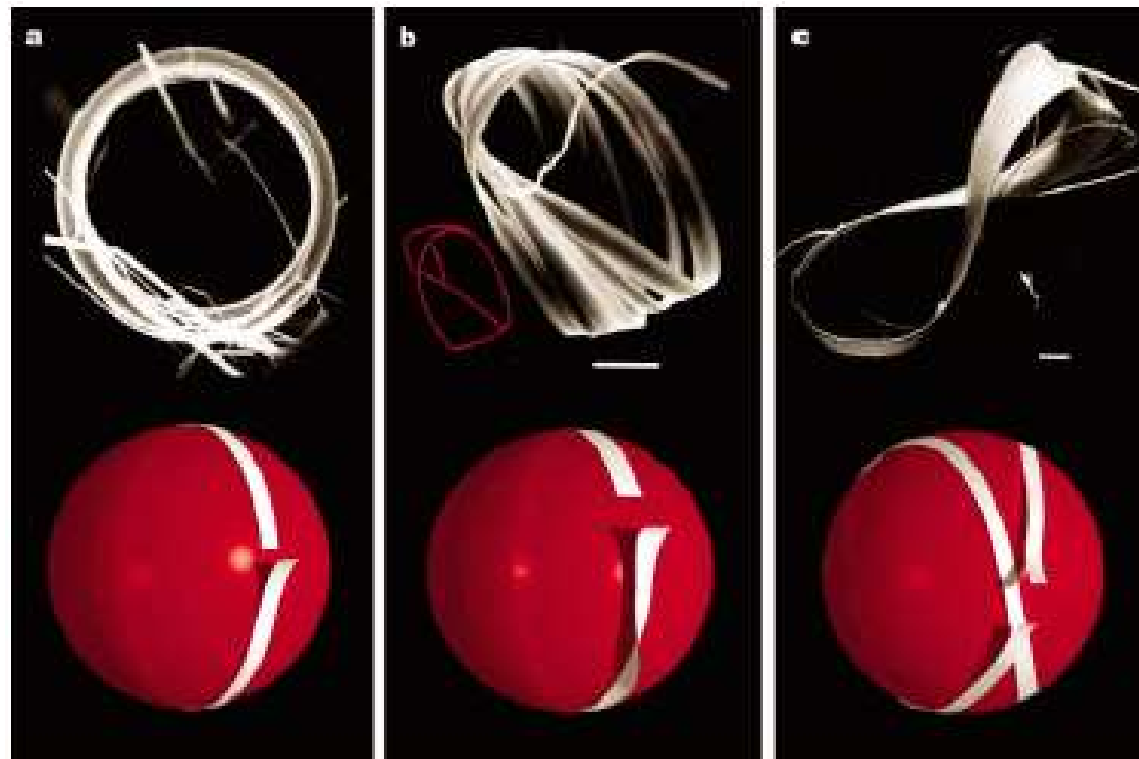


Flux-modified boundary condition:

$$\psi'(\varphi + 2\pi, \zeta) = \boxed{\exp\left(i 2\pi \frac{\Phi}{\Phi_0}\right) \psi'(\varphi, -\zeta)}$$

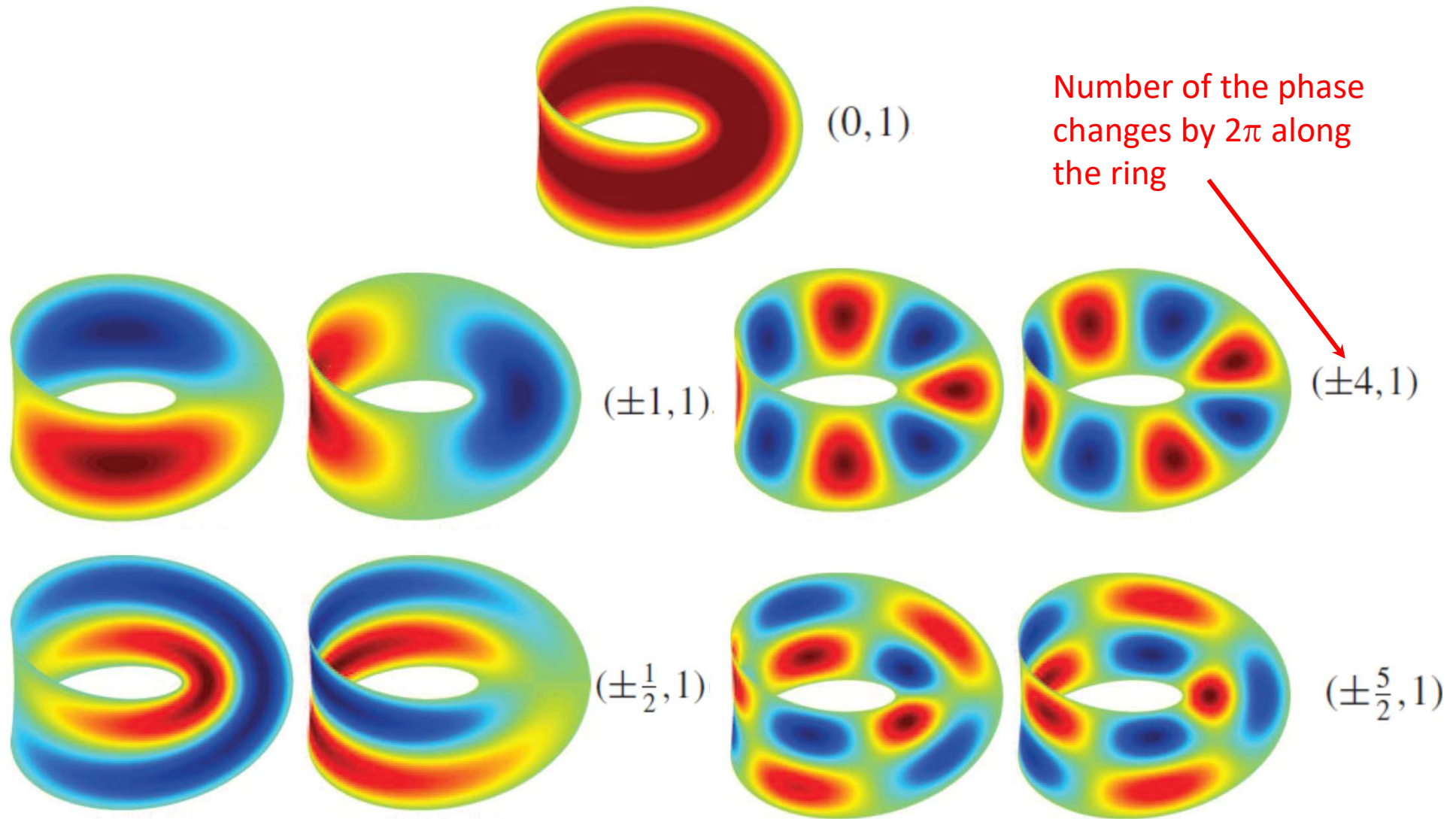
Self-assembly of Möbius strips

Spooling a single crystalline NbSe_3 ribbon on a selenium sphere by surface tension produces a twist leading to formation of a one-sided Möbius strip.



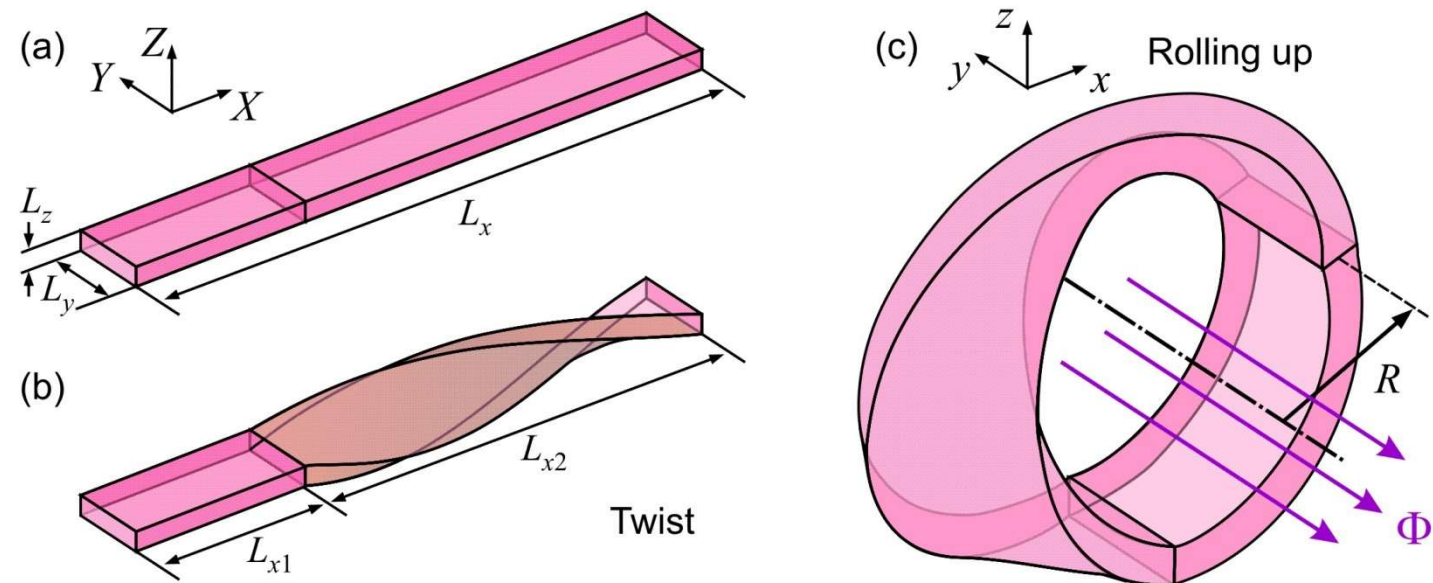
the monoclinic ($P21/m$) crystal symmetry inherent in NbSe_3 induces a twist in the strip when bent
 $D \sim 100 \mu\text{m}$; $w = 1 \mu\text{m}$

Quantum mechanics on a Möbius ring



Z. Li and L. R. Ram-Mohan, Phys. Rev. B 85, 195438 (2012).

Modeling of a Möbius ring with a non-uniform twist



...generates a modification of space metric

$$\mathbf{R}(X, Y, Z) \rightarrow \mathbf{r}(x, y, z)$$

$$\begin{cases} x = (R - Z) \sin \frac{X}{R}, \\ y = Y, \\ z = R - (R - Z) \cos \frac{X}{R} \end{cases} \text{ for } X < L_{x1}; \quad \begin{cases} x = (R - Y \sin \xi - Z \cos \xi) \sin \frac{X}{R}, \\ y = Y \cos \xi - Z \sin \xi, \\ z = R - (R - Y \sin \xi - Z \cos \xi) \cos \frac{X}{R} \end{cases} \text{ for } X > L_{x1},$$

$$R = \frac{L_x}{2\pi}, \quad \xi = \kappa(X - L_{x1}), \quad \kappa = \frac{\pi}{L_{x2}}.$$

$$g_{ij} = \frac{\partial x}{\partial X^i} \frac{\partial x}{\partial X^j} + \frac{\partial y}{\partial X^i} \frac{\partial y}{\partial X^j} + \frac{\partial z}{\partial X^i} \frac{\partial z}{\partial X^j} \quad \text{metric}$$

$$\|g_{ij}\| = \begin{pmatrix} \Phi^2 & 0 & 0 \\ 0 & 1 & 0 \\ 0 & 0 & 1 \end{pmatrix} \Theta(L_{x1} - X) + \begin{pmatrix} \tilde{Y}^2 + \tilde{Z}^2 + \Phi^2 & -\tilde{Z} & \tilde{Y} \\ -\tilde{Z} & 1 & 0 \\ \tilde{Y} & 0 & 1 \end{pmatrix} \Theta(X - L_{x1}),$$

$$\Phi = \left(1 - \frac{Z}{R}\right) \Theta(L_{x1} - X) + \left(1 - \frac{Y}{R} \sin \xi - \frac{Z}{R} \cos \xi\right) \Theta(X - L_{x1}), \quad \tilde{Y} = \kappa Y, \quad \tilde{Z} = \kappa Z$$

$$g = |g_{ij}| = \Phi^2 \quad dx dy dz = \sqrt{g} dX dY dZ = \Phi dX dV dZ$$

$$\psi(\mathbf{r}) = \frac{1}{\sqrt{\Phi}} \chi(\mathbf{R}) \quad \text{norm-conserving transformation}$$

...and a transformation of the Hamiltonian

$$H_0(\{x_i\})\psi = E\psi, H_0(\{x_i\}) = -\frac{\hbar^2}{2m_e}\nabla^2, \nabla^2 = \sum_{i=1}^3 \frac{\partial^2}{\partial x_i^2},$$

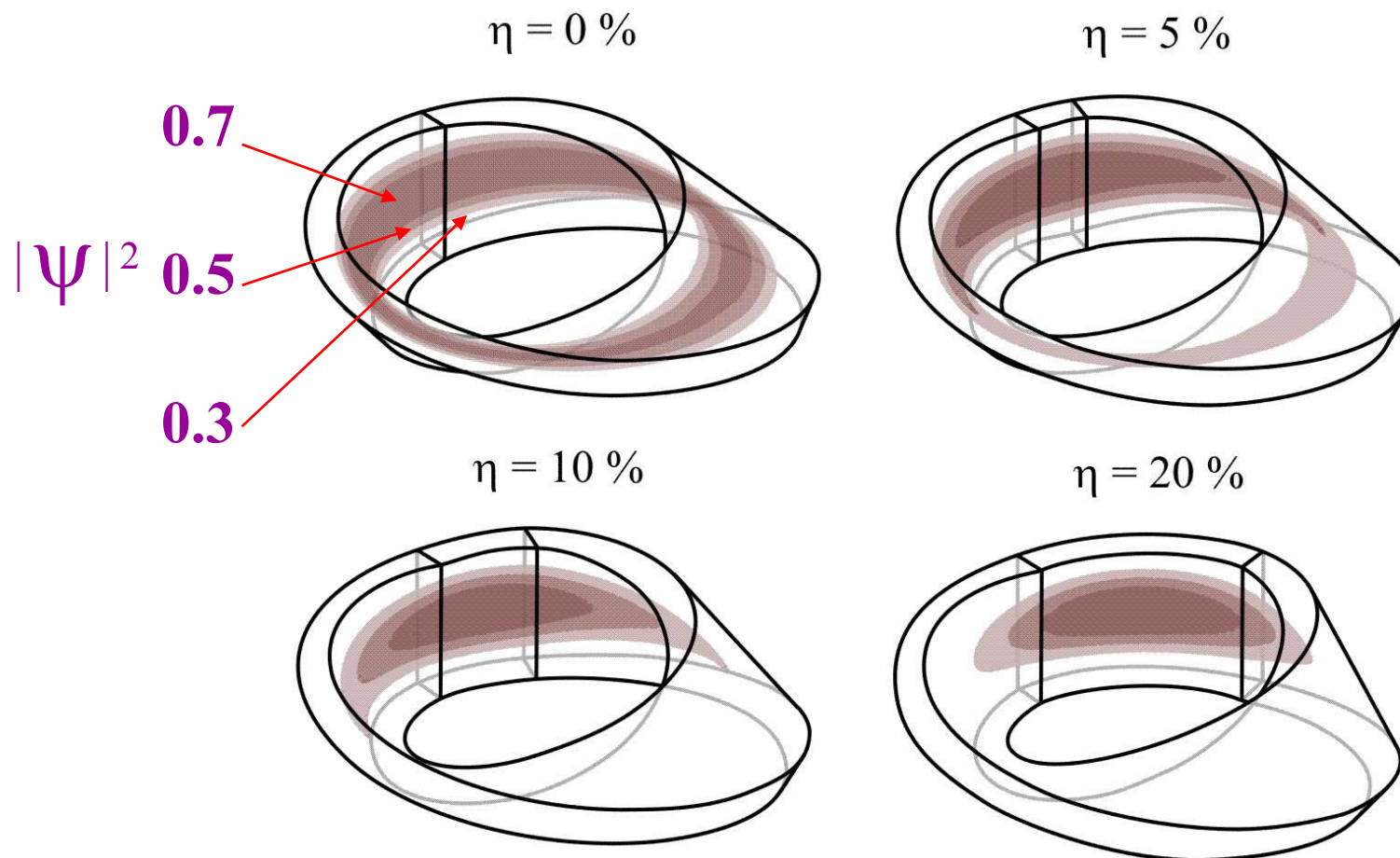
$$\nabla^2\psi = \sum_{i,j=1}^3 \frac{1}{\sqrt{g}} \frac{\partial}{\partial X_i} \left[\sqrt{g} (g^{-1})_{ij} \frac{\partial \psi}{\partial X_j} \right] \quad \text{Laplace-Beltrami operator} \Rightarrow \hat{H}\chi(\mathbf{R}) = E\chi(\mathbf{R})$$

$$\hat{H} = -\frac{\hbar^2}{2m_e} \left[\alpha^{ij} \frac{\partial^2}{\partial X_i \partial X_j} + \beta^i \frac{\partial}{\partial X_i} + \alpha_0 \right]$$

$$\|\alpha^{ij}\| = \begin{pmatrix} 1 & 0 & 0 \\ \Phi^2 & 1 & 0 \\ 0 & 0 & 1 \end{pmatrix} \Theta(L_{x^1} - X) + \begin{pmatrix} \frac{1}{\Phi^2} & \frac{\tilde{Z}}{\Phi^2} & -\frac{\tilde{Y}}{\Phi^2} \\ \frac{\tilde{Z}}{\Phi^2} & \frac{\tilde{Z}^2}{\Phi^2} + 1 & -\frac{\tilde{Y}\tilde{Z}}{\Phi^2} \\ -\frac{\tilde{Y}}{\Phi^2} & -\frac{\tilde{Y}\tilde{Z}}{\Phi^2} & \frac{\tilde{Y}^2}{\Phi^2} + 1 \end{pmatrix} \Theta(X - L_{x^1})$$

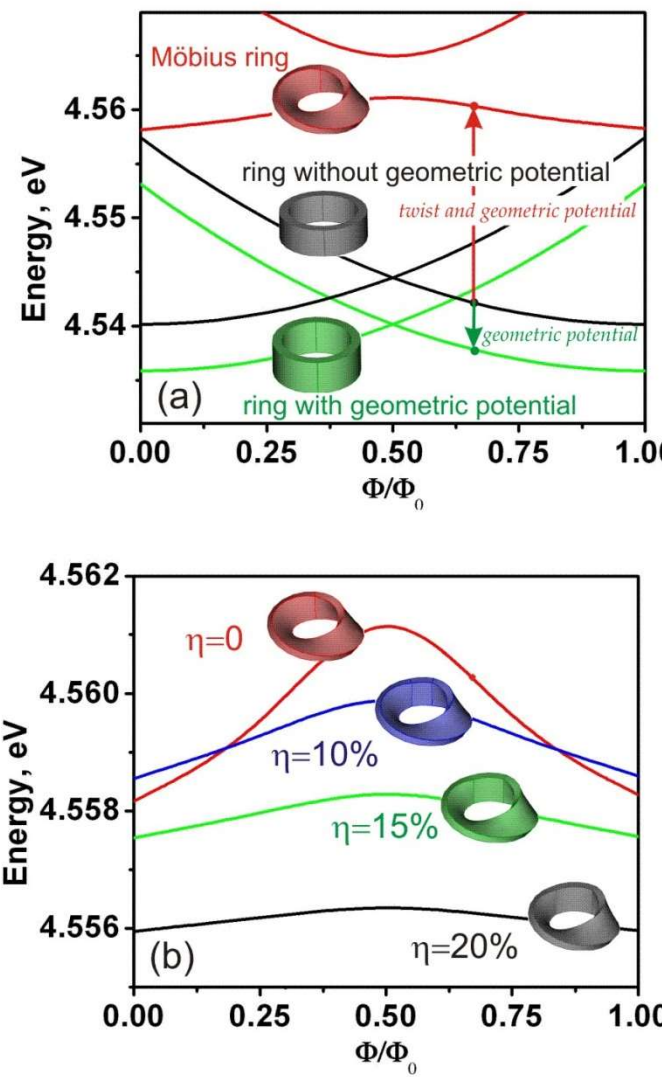
$$(\beta^i) = \left(0, -\frac{\kappa\tilde{Y}}{\Phi^2}, -\frac{\kappa\tilde{Z}}{\Phi^2} \right), \quad \alpha_0 = \frac{1}{4R^2\Phi^2}$$

Localization of electrons in a 3D Möbius ring



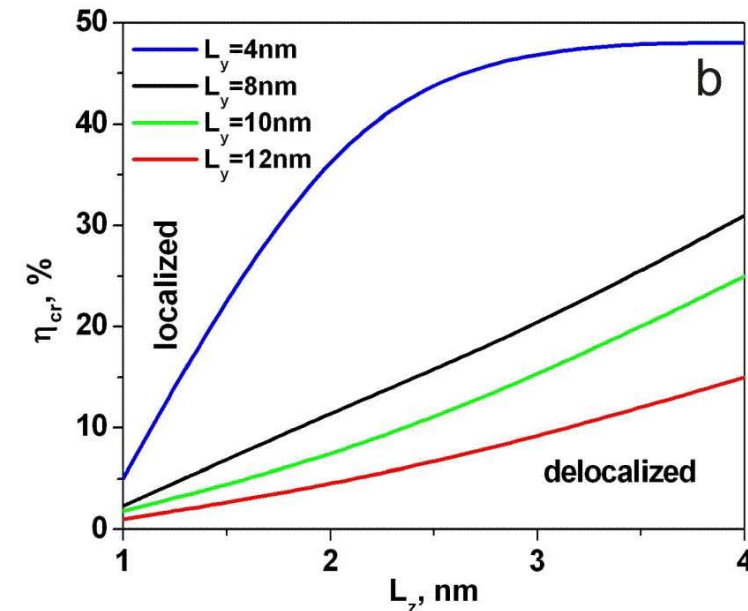
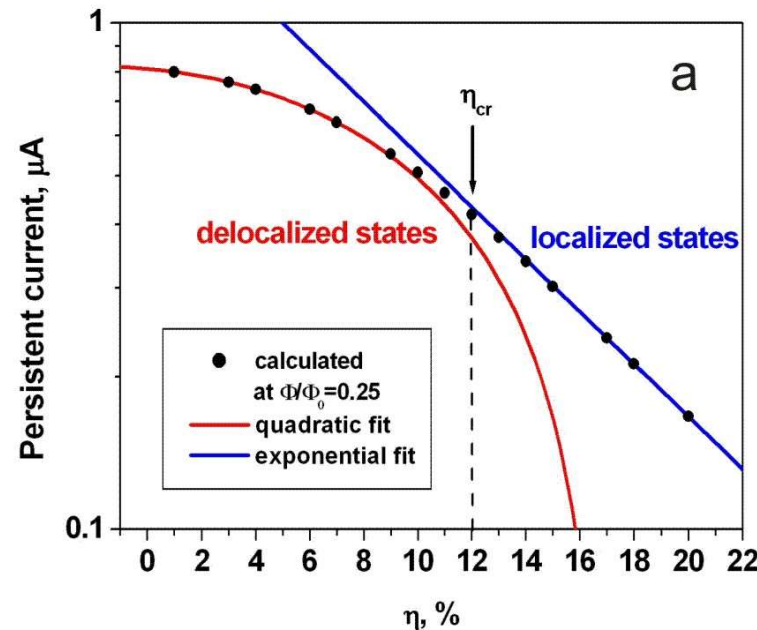
V. M. Fomin, S. Kiravittaya, and O. G. Schmidt, Phys. Rev. B 86, 195421 (2012).

Electron energies in a 3D Möbius ring



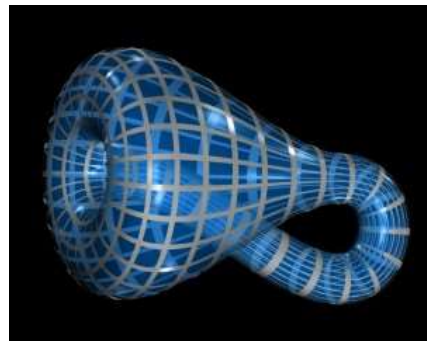
Aharanov-Bohm effect in a 3D Möbius ring

$$I_n(\Phi) = -dE_n(\Phi) / d\Phi$$



V. M. Fomin, S. Kiravittaya, and O. G. Schmidt, Phys. Rev. B 86, 195421 (2012).

A closed Universe



a is the size of the Universe

globally hyperbolic spacetime homeomorphic to $S^1 \times \mathbb{R}^3$

massless scalar field: $\left(-\frac{\partial^2}{\partial t^2} + \frac{\partial^2}{\partial \mathbf{r}^2} \right) G(x, x') = -\delta(x - x').$

Untwisted: periodicity

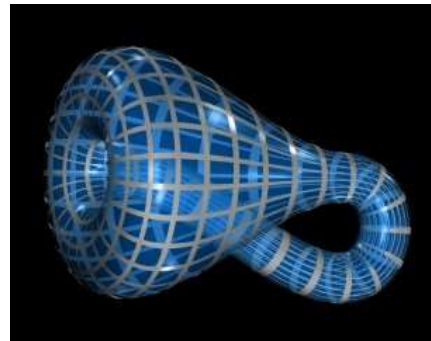
$$G(x, x') = \sum_{n \neq 0} G_0(x, x' + nae_3)$$

Twisted: antiperiodicity

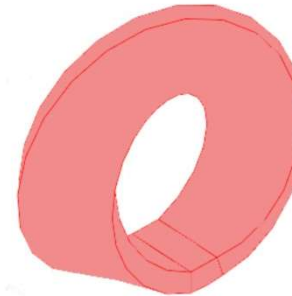
$$G(x, x') = \sum_{n \neq 0} (-1)^n G_0(x, x' + nae_3),$$

B. S. DeWitt, C. F. Hart, C. J. Isham, Physica 96A, 197 (1979).

Verification of the effect of Möbiosity



The closed in itself Universe



Möbius ring

$$\Delta E = 4.5 \times 10^{-3} \text{ eV}$$

$$V = 2\pi \times 10 \times 1 \times 4 = 250 \text{ nm}^3$$
$$\approx 2.5 \times 10^{-25} \text{ m}^3$$

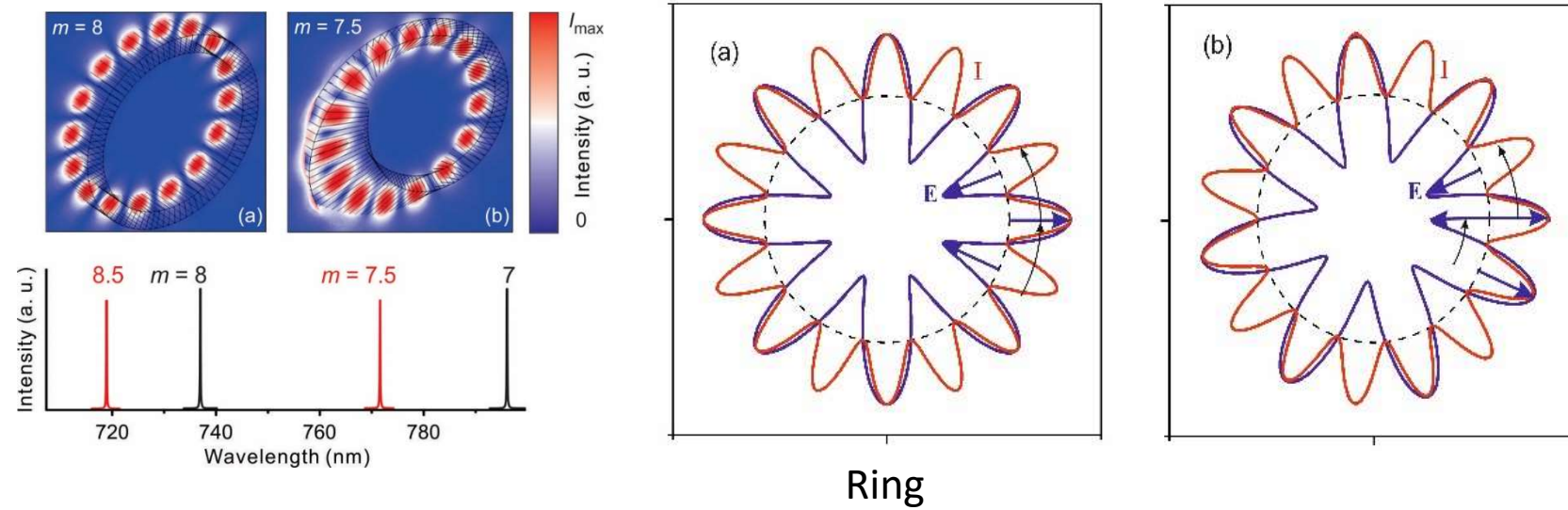
$$\Delta_{twist} \langle T^{00} \rangle = \frac{15}{8} \frac{\pi^2}{90a^4}$$
$$\approx 6 \times 10^{-118} \frac{\text{eV}}{\text{m}^3}$$

$$\frac{\Delta E}{V} \approx 2 \times 10^{22} \frac{\text{eV}}{\text{m}^3}$$

3. TOPOLOGIC STATES OF LIGHT IN MICROCAVITIES

Resonant modes of light in a Möbius-ring resonator

- Möbiosity introduces a key property of fermions to the bosonic electromagnetic field



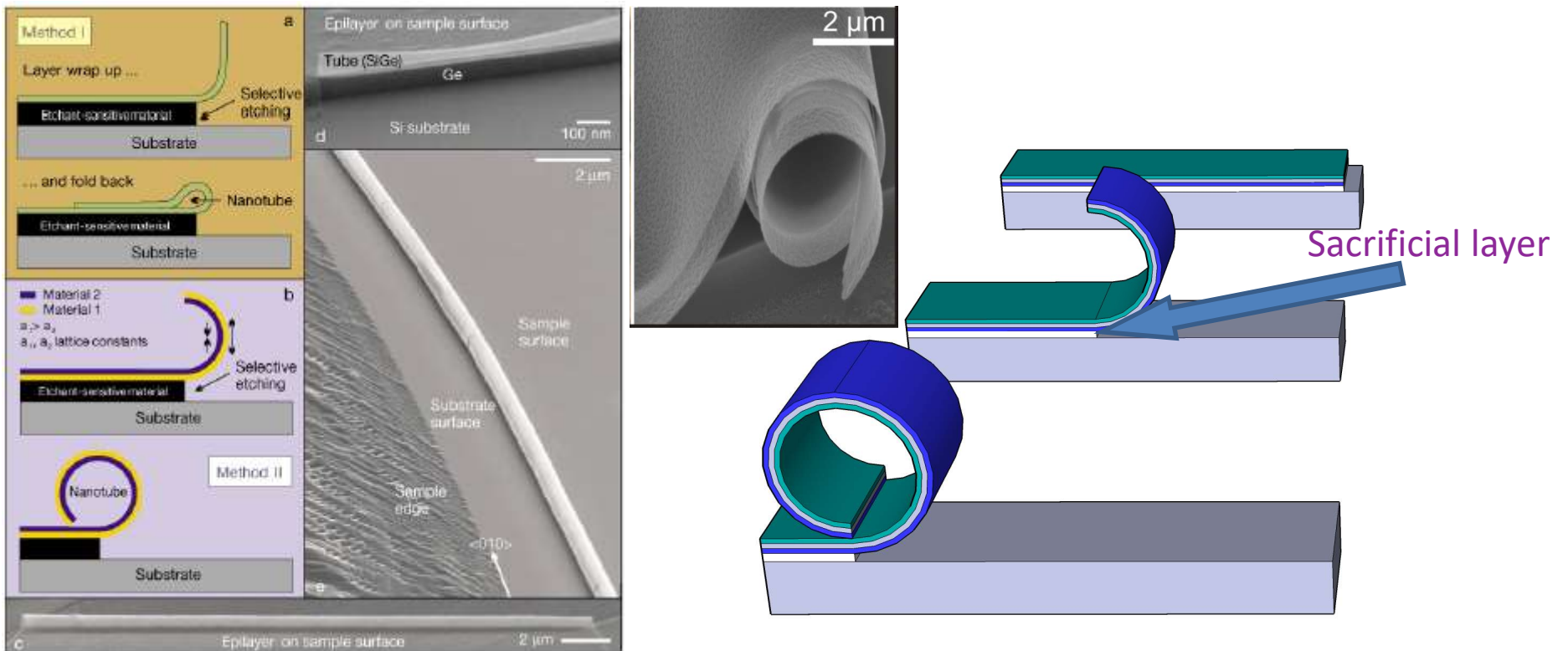
$$\mathbf{E}(u + 2\pi) = \mathbf{E}(u)$$

Möbius ring

$$\mathbf{E}(u + 2\pi) = -\mathbf{E}(u), \mathbf{E}(u + 4\pi) = \mathbf{E}(u)$$

S. L. Li, L. B. Ma, V. M. Fomin, S. Böttner, M. R. Jorgensen, and O. G. Schmidt,
arXiv: 1311.7158 [physics.optics], 1-9 (2013).

Self-organization of nanostructures – rolled-up nanotubes



V. Ya. Prinz et al., Physica E 6, 828 (2000)

O. G. Schmidt and K. Eberl, Nature 410, 168 (2001)

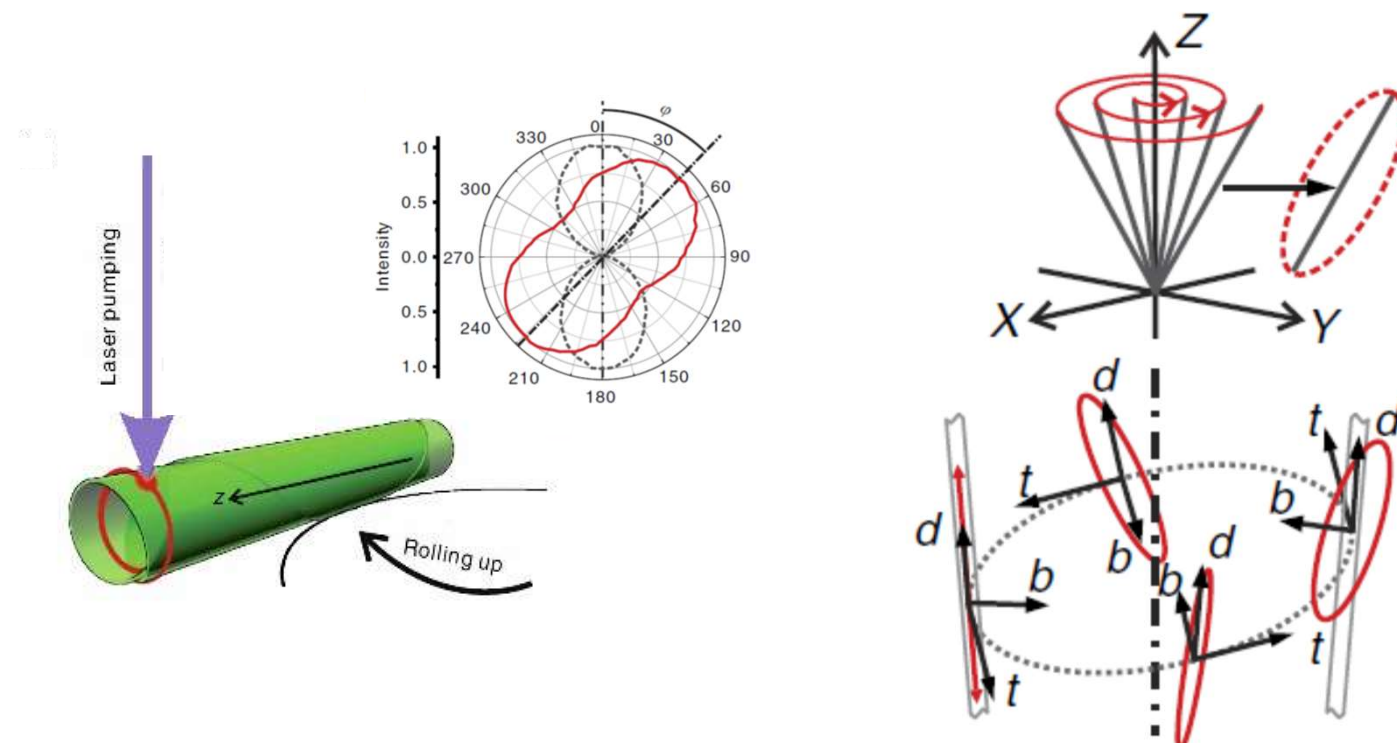
D. J. Thurmer, C. C. Bof Bufon, C. Deneke and O. G. Schmidt, Nano Lett. 10, 3704 (2010)

D. D. Karnaushenko, D. Karnaushenko, D. Makarov, O. G. Schmidt, NPG Asia Mater. 7, e188 (2015)

Optical spin-orbit coupling in asymmetric microcavities

Self-organization in nanostructures – rolled-up cavities

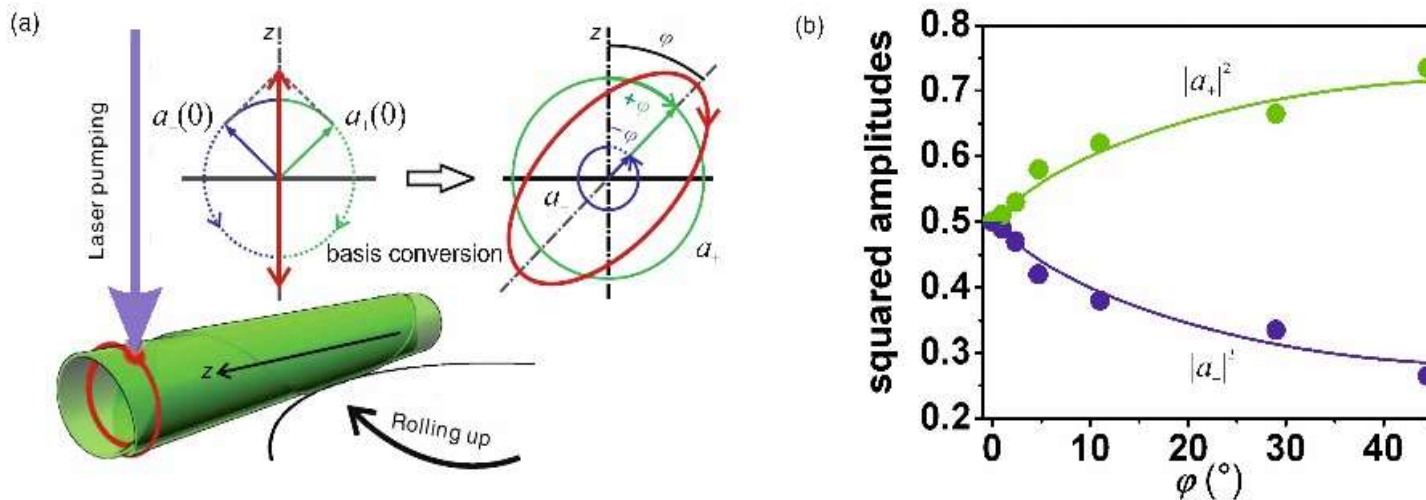
- rolled-up high-tech enables optical spin-orbit coupling in asymmetric microcavities
- observation of a non-cyclic optical geometric phase acquired in a non-Abelian evolution



L. B. Ma, S. L. Li, V. M. Fomin, M. Hentschel, J. B. Götte, Y. Yin, M. R. Jorgensen, and O. G. Schmidt, Nature Communications 7, 10983 (2016).

Optical spin-orbit coupling in asymmetric microcavities

- observation of a non-cyclic optical geometric phase acquired in a non-Abelian evolution
- theoretical explanation of the non-Abelian optical polarization evolution



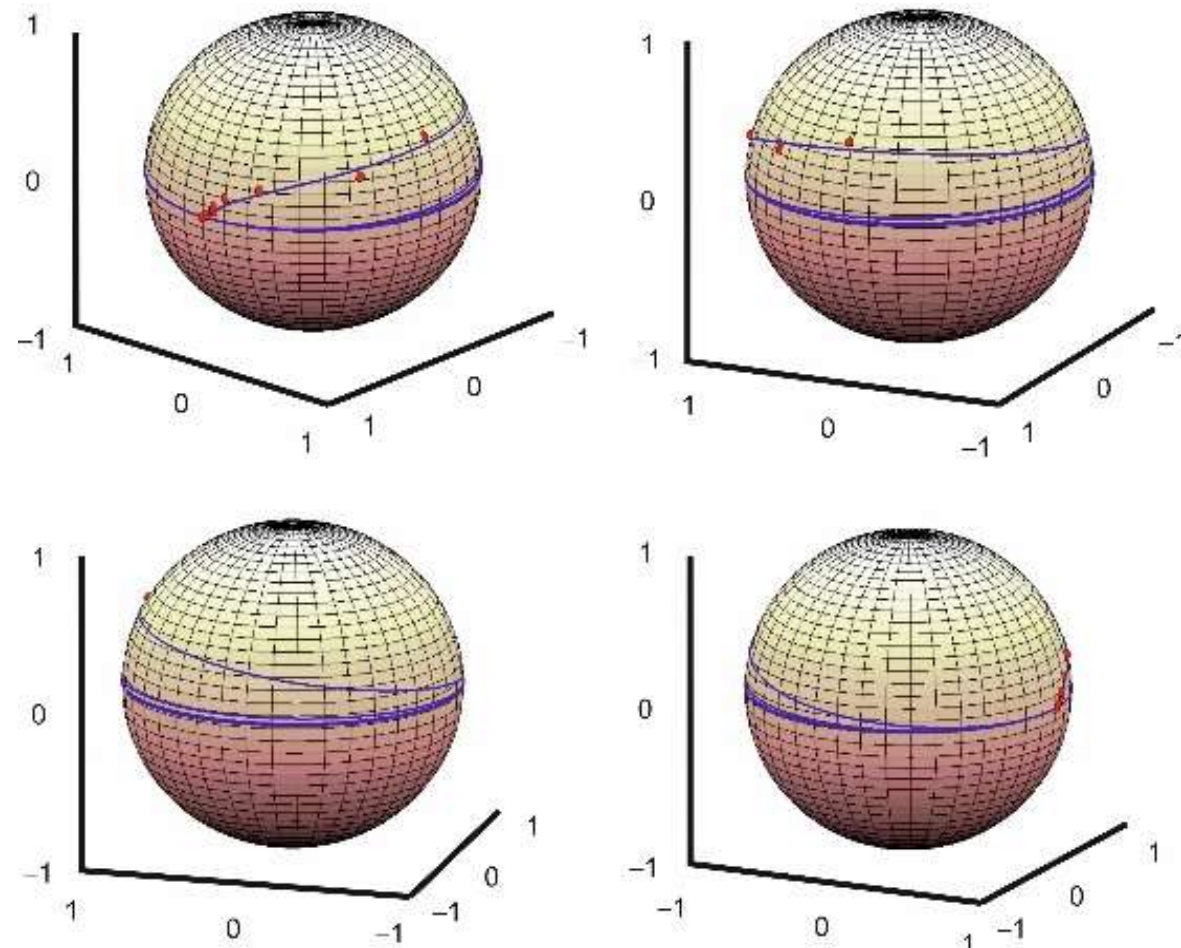
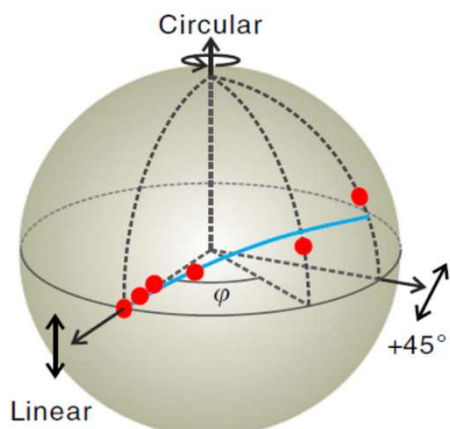
$$\mathbf{a} = \begin{pmatrix} a_+ \\ a_- \end{pmatrix} = \exp \begin{pmatrix} -i\varphi & iC_A \\ iC_A & i\varphi \end{pmatrix} \frac{1}{\sqrt{2}} \begin{pmatrix} 1 \\ 1 \end{pmatrix} = \frac{1}{\sqrt{2}} \begin{pmatrix} \cos \sqrt{\varphi^2 + C_A^2} + i(\varphi - C_A) \frac{\sin \sqrt{\varphi^2 + C_A^2}}{\sqrt{\varphi^2 + C_A^2}} \\ \cos \sqrt{\varphi^2 + C_A^2} + i(\varphi + C_A) \frac{\sin \sqrt{\varphi^2 + C_A^2}}{\sqrt{\varphi^2 + C_A^2}} \end{pmatrix}$$

L. B. Ma, S. L. Li, V. M. Fomin, M. Hentschel, J. B. Götte, Y. Yin, M. R. Jorgensen, and O. G. Schmidt, Nature Communications 7, 10983 (2016).

Optical spin-orbit coupling in asymmetric microcavities

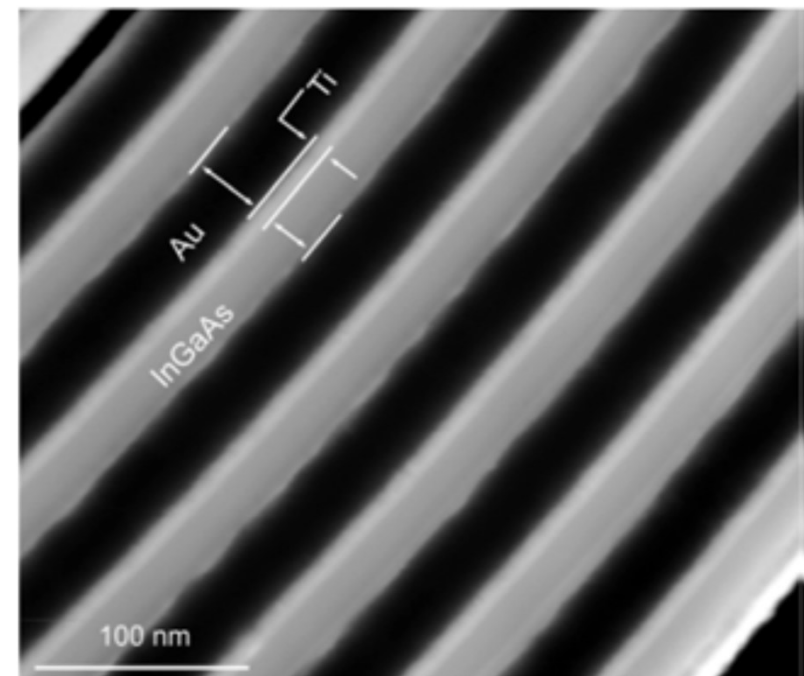
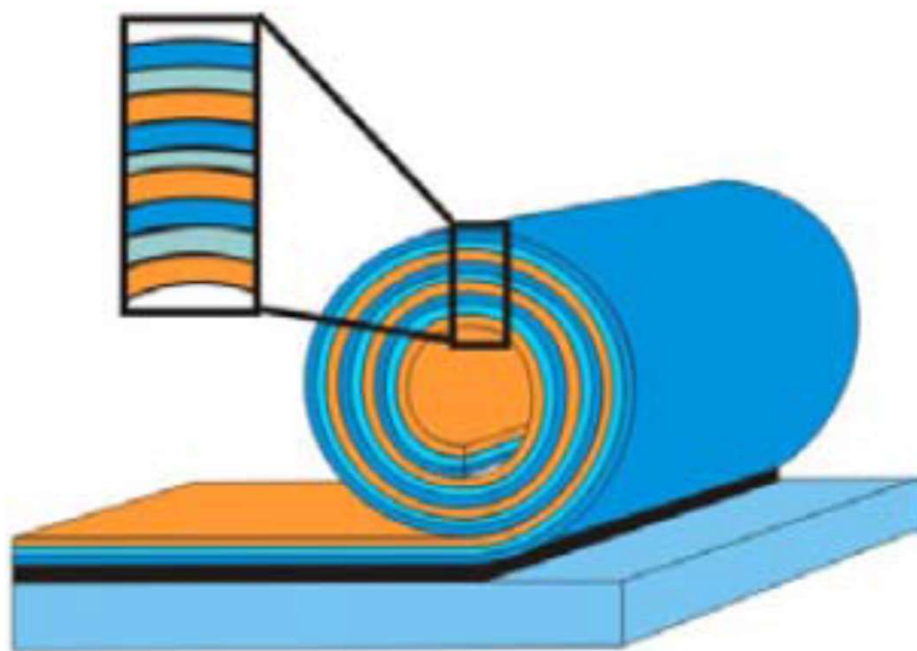
- Plot of the non-Abelian evolution as a curve on the Poincaré sphere

$$C_A = 0.318 \times \varphi^{-0.433}$$



L. B. Ma, S. L. Li, V. M. Fomin, M. Hentschel, J. B. Götte, Y. Yin, M. R. Jorgensen, and O. G. Schmidt, Nature Communications 7, 10983 (2016).

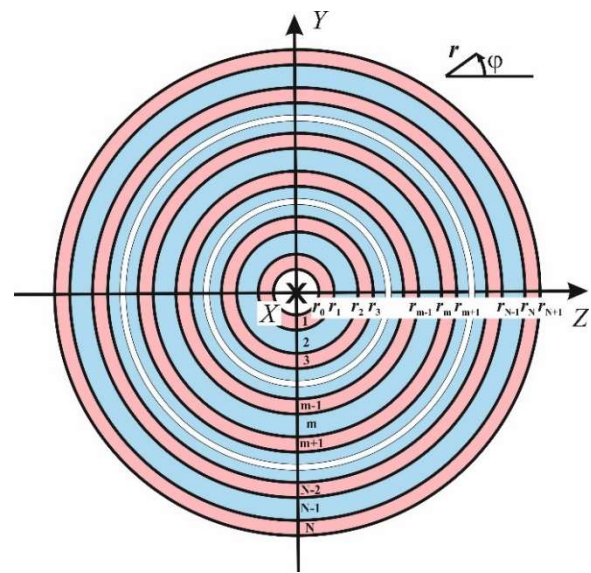
4. Phononic multishell metamaterials



Au/Ti/InGaAs

C. Deneke, R. Songmuang, N. Y. Jin-Phillipp, O. G. Schmidt,
J. Phys. D, 42, 103001 (2009).

Theoretical model



$$\mu_m \nabla^2 \mathbf{u}_m + (\lambda_m + \mu_m) \nabla \nabla \cdot \mathbf{u}_m = \rho_m \frac{\partial^2 \mathbf{u}_m}{\partial t^2}$$

At every intershell boundary r_m , ($m = 1, \dots, N-1$)

$$\sigma_{rrm} = \sigma_{rrm+1}; \quad u_{rm} = u_{rm+1};$$

$$\sigma_{rxm} = \sigma_{rxm+1}; \quad u_{xm} = u_{xm+1};$$

$$\sigma_{r\phi m} = \sigma_{r\phi m+1}; \quad u_{\phi m} = u_{\phi m+1}.$$

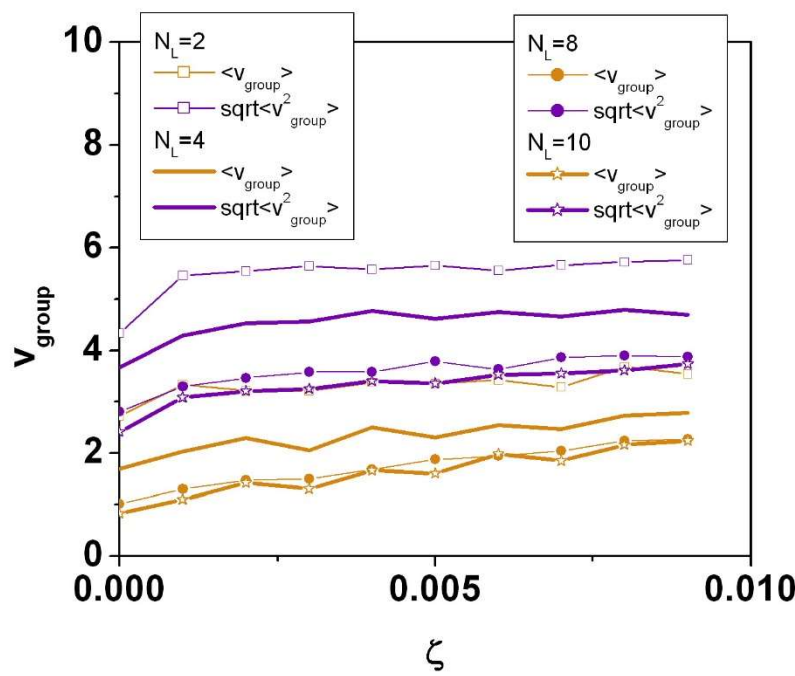
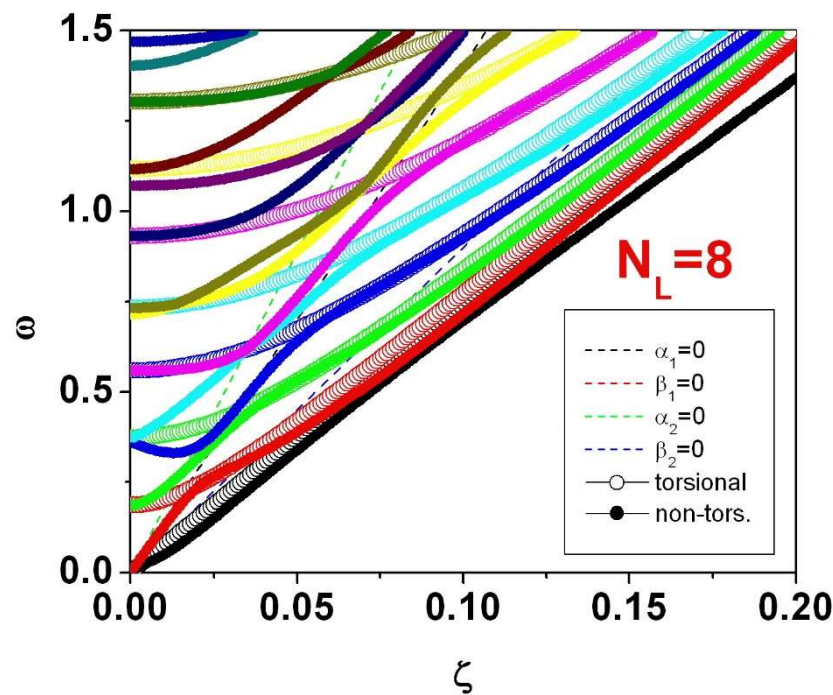
At the internal boundary r_0 , at the external boundary r_N ,

$$0 = \sigma_{rr1}; \quad \sigma_{rrN} = 0;$$

$$0 = \sigma_{r1}; \quad \sigma_{rxN} = 0;$$

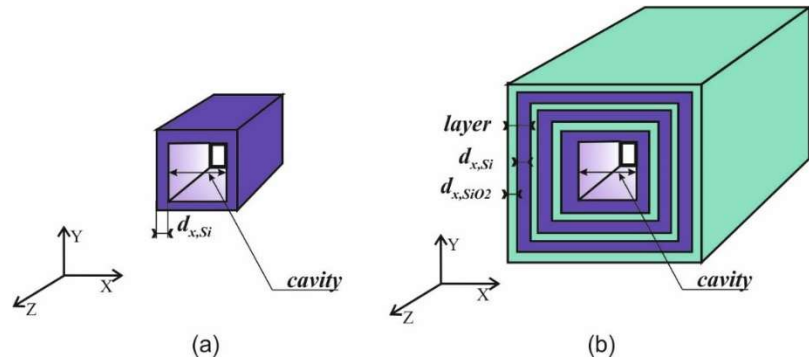
$$0 = \sigma_{r\phi 1}. \quad \sigma_{r\phi N} = 0.$$

Phonon energy spectra for Si/SiO₂ multishells



Atomistic analysis of phonons in Si/SiO₂ Nanotubes

Lattice Dynamics



$$m\omega^2 w_i(\vec{n}; \vec{q}) = \sum_{j=1,2,3} \sum_{\vec{n}'} D_{ij}(\vec{n}, \vec{n}'; \vec{q}) w_j(\vec{n}'; \vec{q})$$

$D_{ij} = \Phi_{ij}(\vec{n}, \vec{n}') \exp(i\vec{q} \times (\vec{n}' - \vec{n}))$ - components of the dynamic matrix

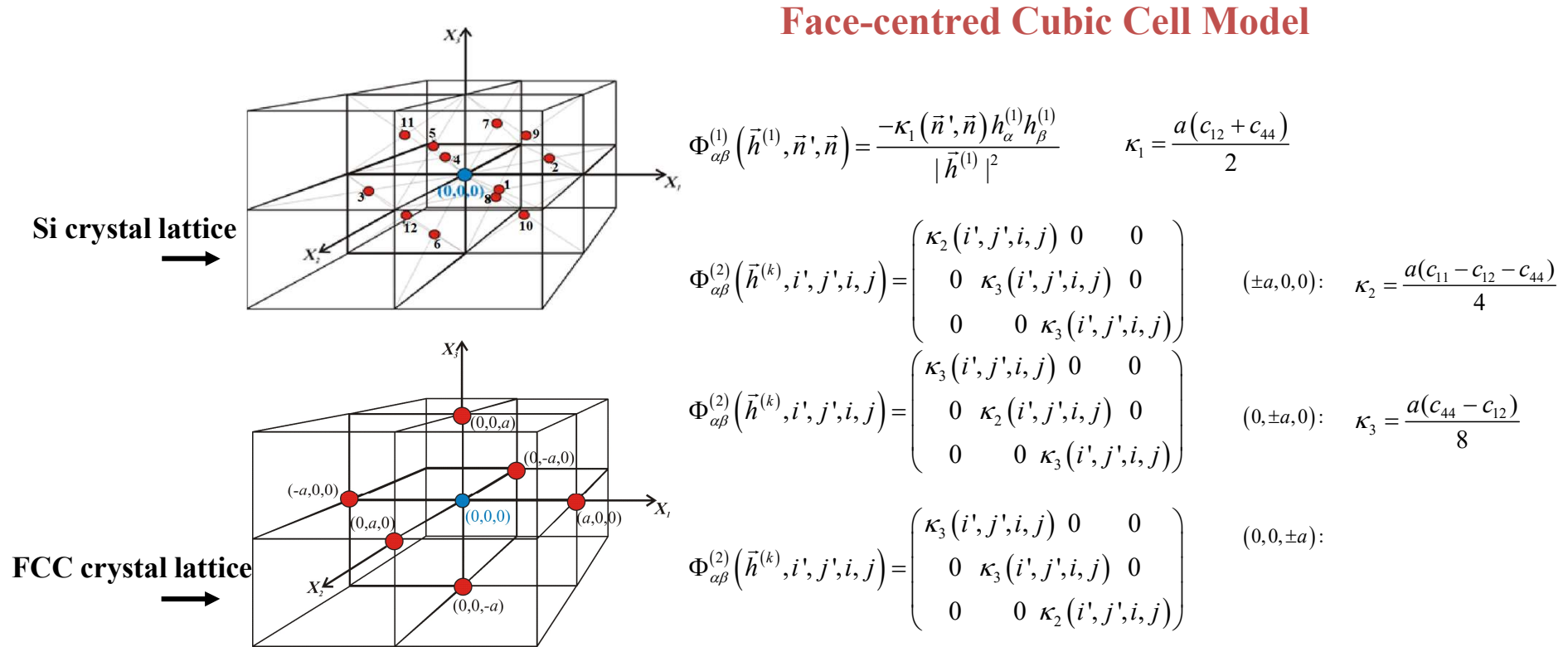
w_i - i -th component of the atomic displacement

ω - phonon frequencies, \vec{q} - wave vector,

m - mass of an atom

M. Born and Th. von Kàrmà̄n, Physikalische Zeitschrift 13, 297 (1912)
M.T. Dove, Introduction to the theory of lattice dynamics, Collection
Société Française de la Neutronique 12, 123 (2011)

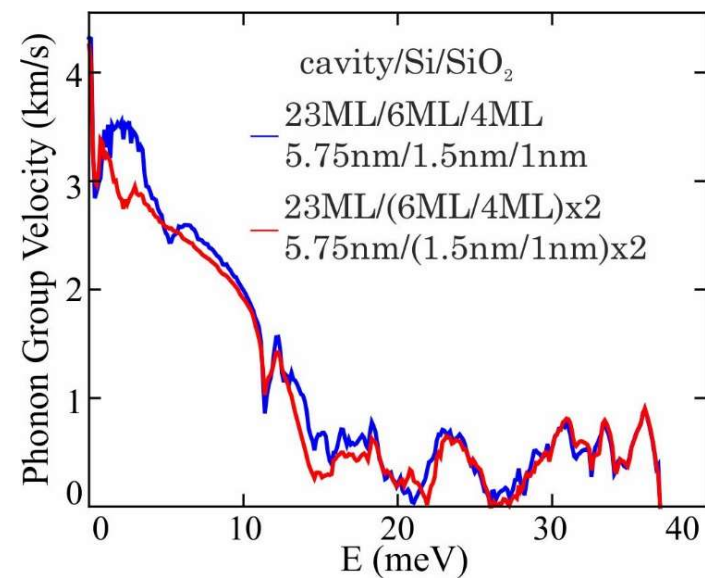
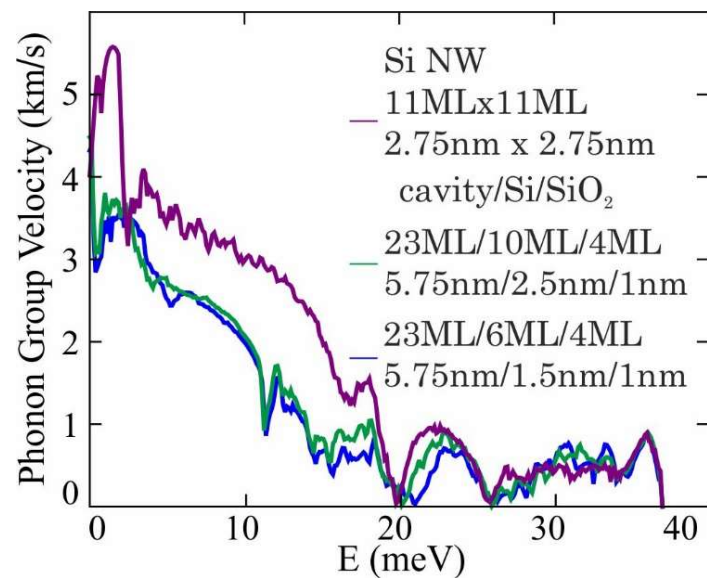
Lattice Dynamics



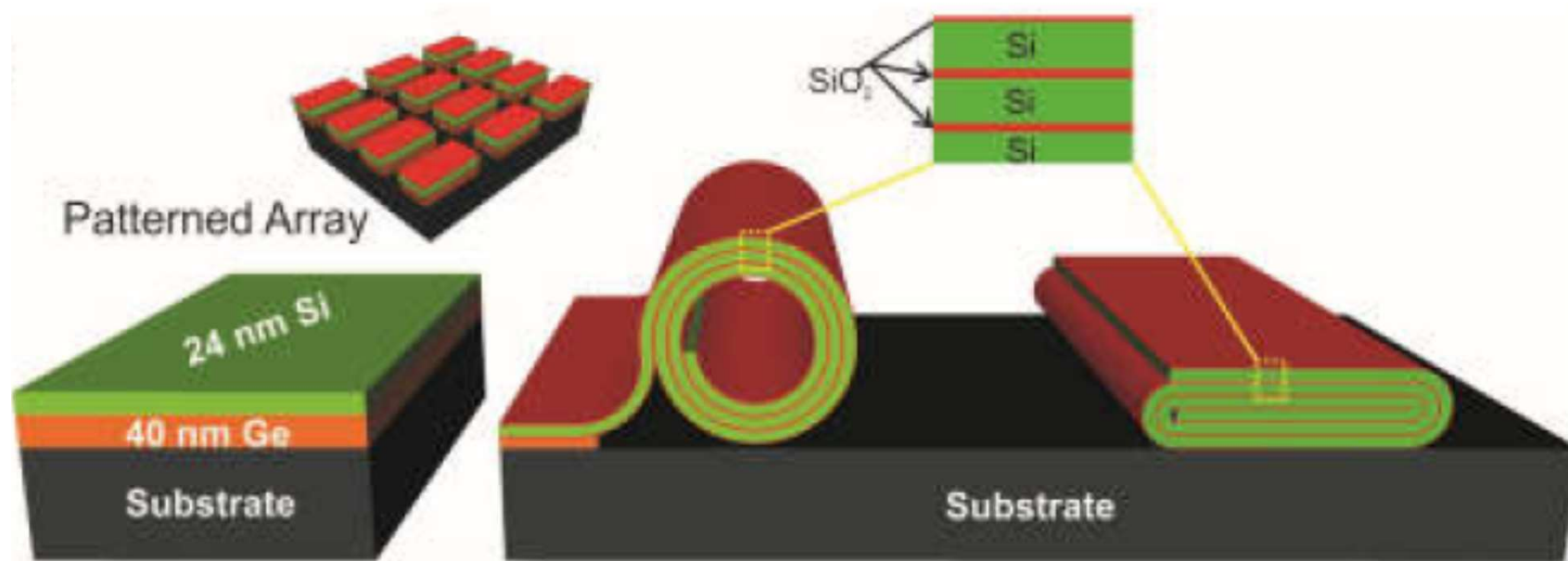
S. Tamura, Y. Tanaka, H. Maris, Physical Review B, 60, 2627 (1999)

D.L. Nika, A.I.Cocemasov, C.I. Isacova, A.A. Balandin, V.M. Fomin and O.G. Schmidt Phys. Rev. B 85, 205439 (2012).

Reduction of Phonon Group Velocities in Si/SiO₂ NTs

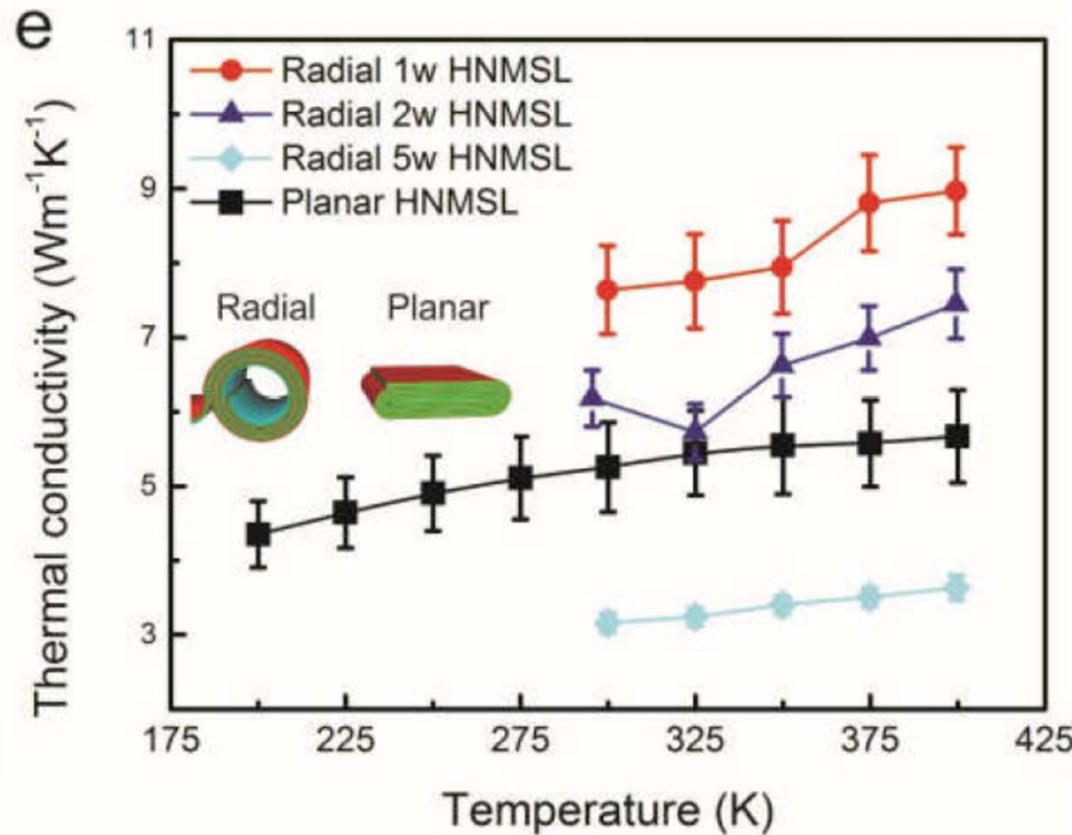


In-Plane Thermal Conductivity of Radial and Planar Si/SiO_x Hybrid Nanomembrane Superlattices



G. Li, M. Yarali, A. Cocemasov, S. Baunack, D. L. Nika, V. M. Fomin, S. Singh, T. Gemming, F. Zhu, A. Mavrokefalos, O. G. Schmidt, ACS Nano 11, 8215 (2017).

Experimental In-Plane Thermal Conductivity of Radial and Planar Si/SiO_x Hybrid Nanomembrane Superlattices



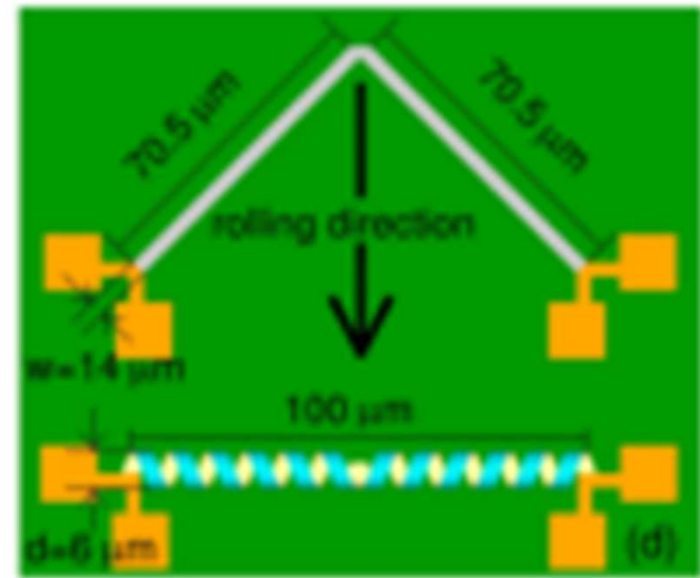
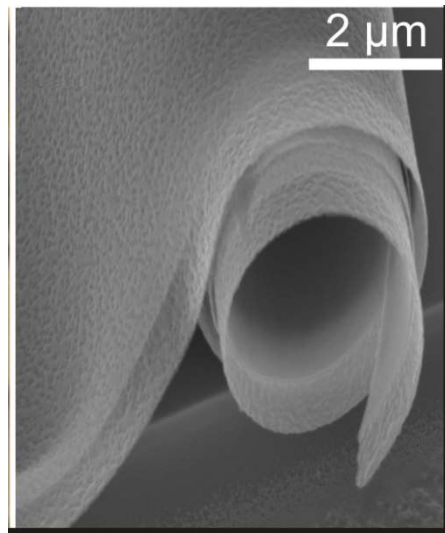
The thermal inter-correlation between Si layers implies the superlattice features of the fabricated structures.

G. Li, M. Yarali, A. Cocemasov, S. Baunack, D. L. Nika, V. M. Fomin, S. Singh, T. Gemming, F. Zhu, A. Mavrokefalos, O. G. Schmidt, ACS Nano 11, 8215–8222 (2017).

5. Geometry-driven effects in superconductor nanoarchitectures

Superconductor microarchitectures

Trilayers InGaAs/GaAs/Nb



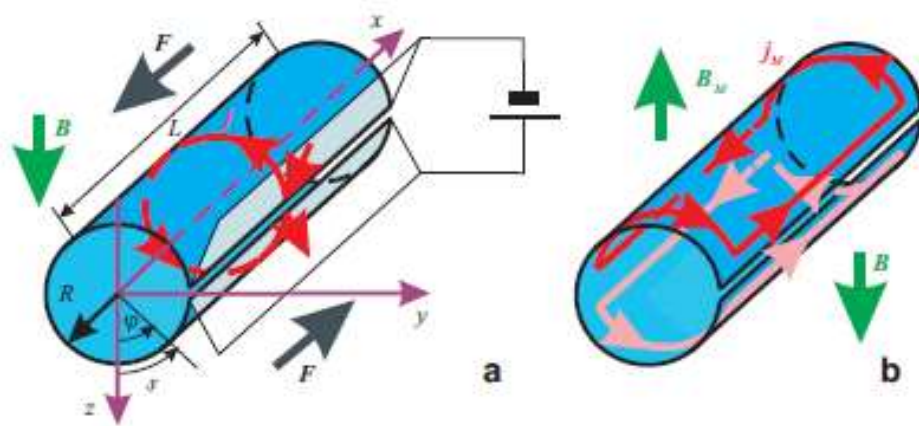
D. J. Thurmer, C. Deneke, and O. G. Schmidt, J. Phys. D: Appl. Phys. 41 205419 (2008).

D. J. Thurmer, C. C. B. Bufon, C. Deneke, and O. G. Schmidt, Nano Lett. 10 3704 (2010).

V. M. Fomin, R. O. Rezaev, E. A. Levchenko, D. Grimm and O. G. Schmidt,
Journal of Physics: Condensed Matter 29, 395301 (2017).

S. Löscher, A. Alfonsov, O. V. Dobrovolskiy, R. Keil, V. Engemaler, S. Baunack,
G. Li, O. G. Schmidt and D. Bürger, ASC Nano 13, 2948 (2019).

3. Superconductivity in open tubes



$$\frac{\partial \psi}{\partial t} = (\nabla - i\mathbf{A})^2 \psi + 2\kappa^2 \psi (1 - |\psi|^2)$$

$$(\nabla - i\mathbf{A})\psi|_{n,\text{boundary}} = 0;$$

$$\left[\nabla - i\left(\mathbf{A} + \mathbf{j}/|\psi|^2 \right) \right] \psi|_{n,\text{electrode}} = 0.$$

$$\mathbf{A} = A \mathbf{e}_x, A = -By$$

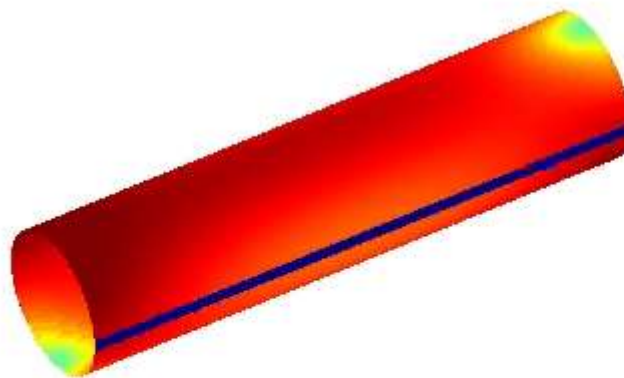
$$B_n(\varphi) = -B \sin(\varphi)$$

$$\Phi = 2RLB$$

- (a) Scheme of the structure.**
- (b) Scheme of Meissner currents in a superconducting tube.**

V. M. Fomin, R. O. Rezaev, and O. G. Schmidt, Nano Lett. **12** 1282 (2012).

Vortex Dynamics



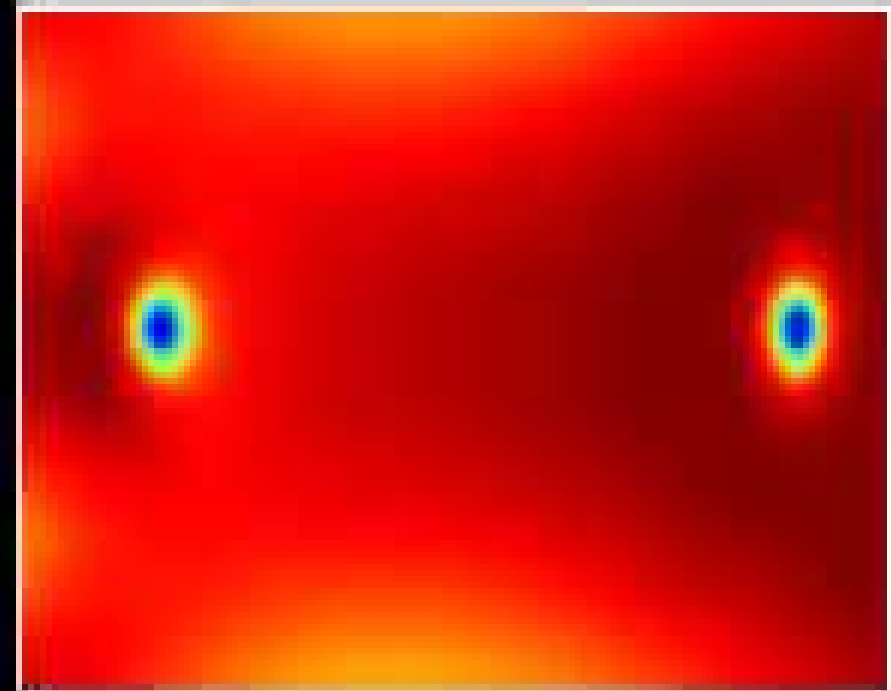
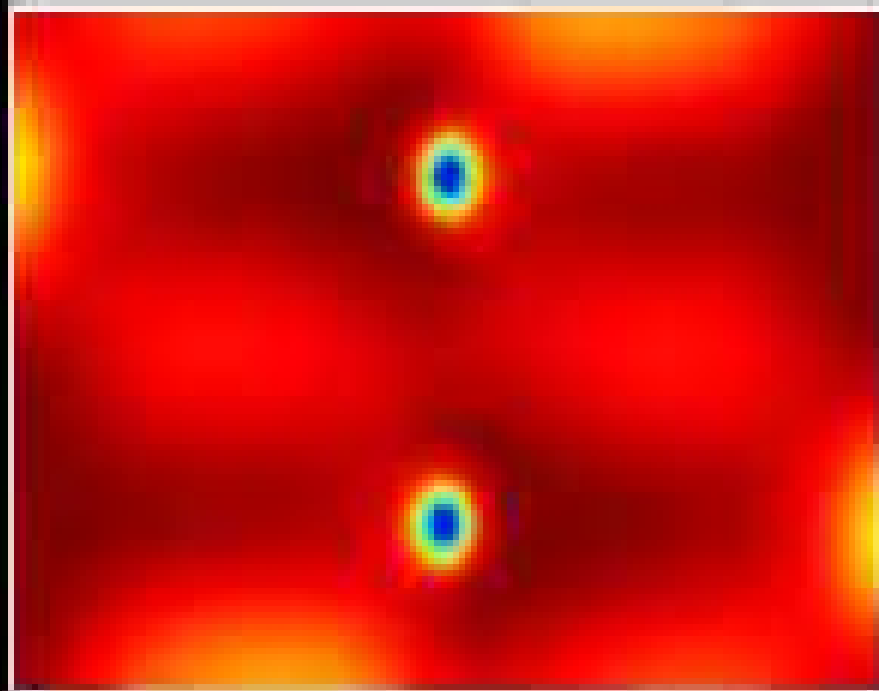
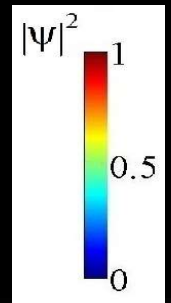
The sparse-vortex regime for a Nb tube of radius $R = 500$ nm and length $L = 3.5$ μm with a slit of width $1/30 \times 2\pi R = 105$ nm at $\Phi/\Phi_0 = 7.5$.

$$\mathbf{F} = \mathbf{j}_{tot} \times \mathbf{B} \quad \mathbf{j}_{tot} = \mathbf{j} + \mathbf{j}_M + \mathbf{j}_{vortices}$$

Unrolled surface of a tube

Planar film

Transport current

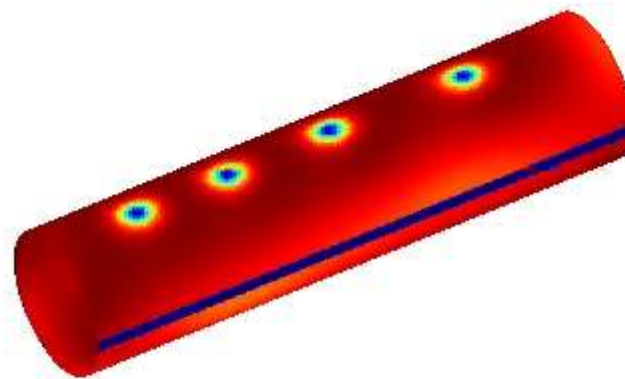


Length = 3.5 μm ; Magnetic field = 8.8 mT;
Radius of a tube = 280 nm

Length = 3.5 μm ; Magnetic field = 3.5 mT;
Height = $2\pi \times \text{Radius}$

Process time = 10 ns

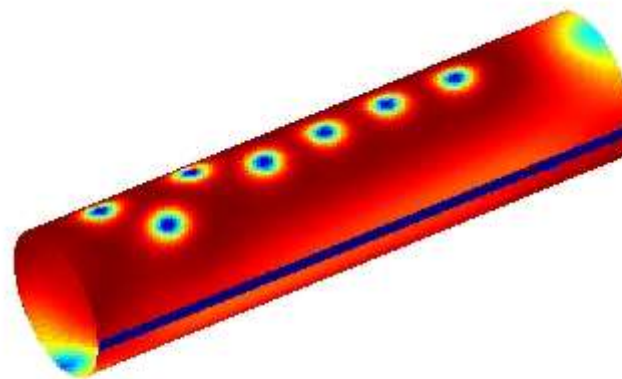
Vortex Dynamics



The multi-vortex regime for a Nb tube of radius $R = 500$ nm and length $L = 3.5$ μm with a slit of width $1/30 \times 2\pi R = 105$ nm at $\Phi/\Phi_0 = 11$.

$$\mathbf{F} = \mathbf{j}_{tot} \times \mathbf{B} \quad \mathbf{j}_{tot} = \mathbf{j} + \mathbf{j}_M + \mathbf{j}_{vortices}$$

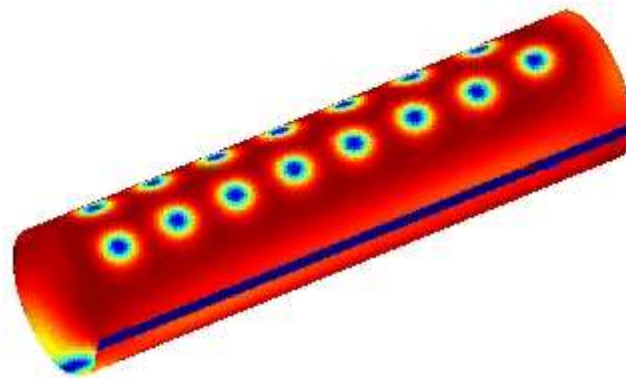
Vortex Dynamics



The multi-vortex regime for a Nb tube of radius $R = 500$ nm and length $L = 3.5$ μm with a slit of width $1/30 \times 2\pi R = 105$ nm at $\Phi/\Phi_0 = 15$.

$$\mathbf{F} = \mathbf{j}_{tot} \times \mathbf{B} \quad \mathbf{j}_{tot} = \mathbf{j} + \mathbf{j}_M + \mathbf{j}_{vortices}$$

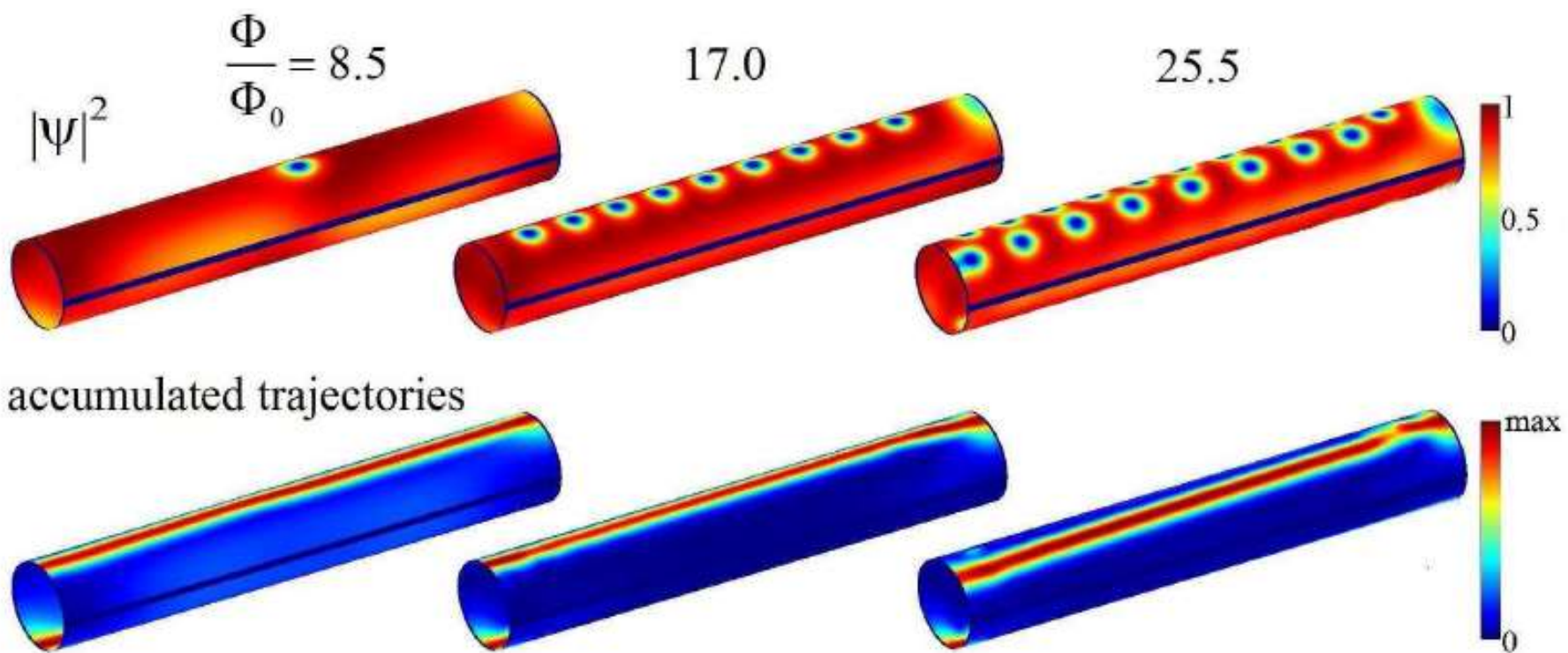
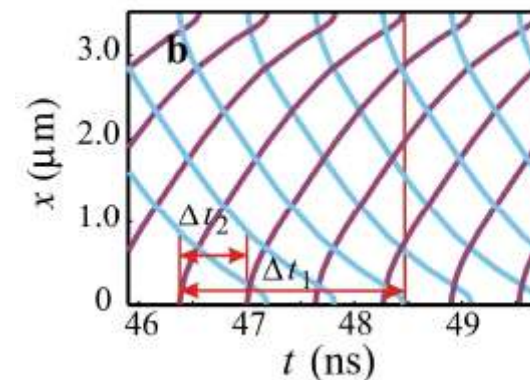
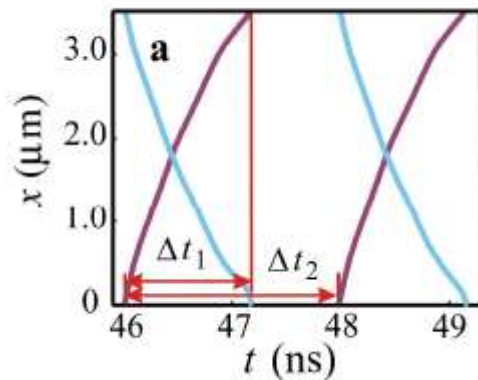
Vortex Dynamics



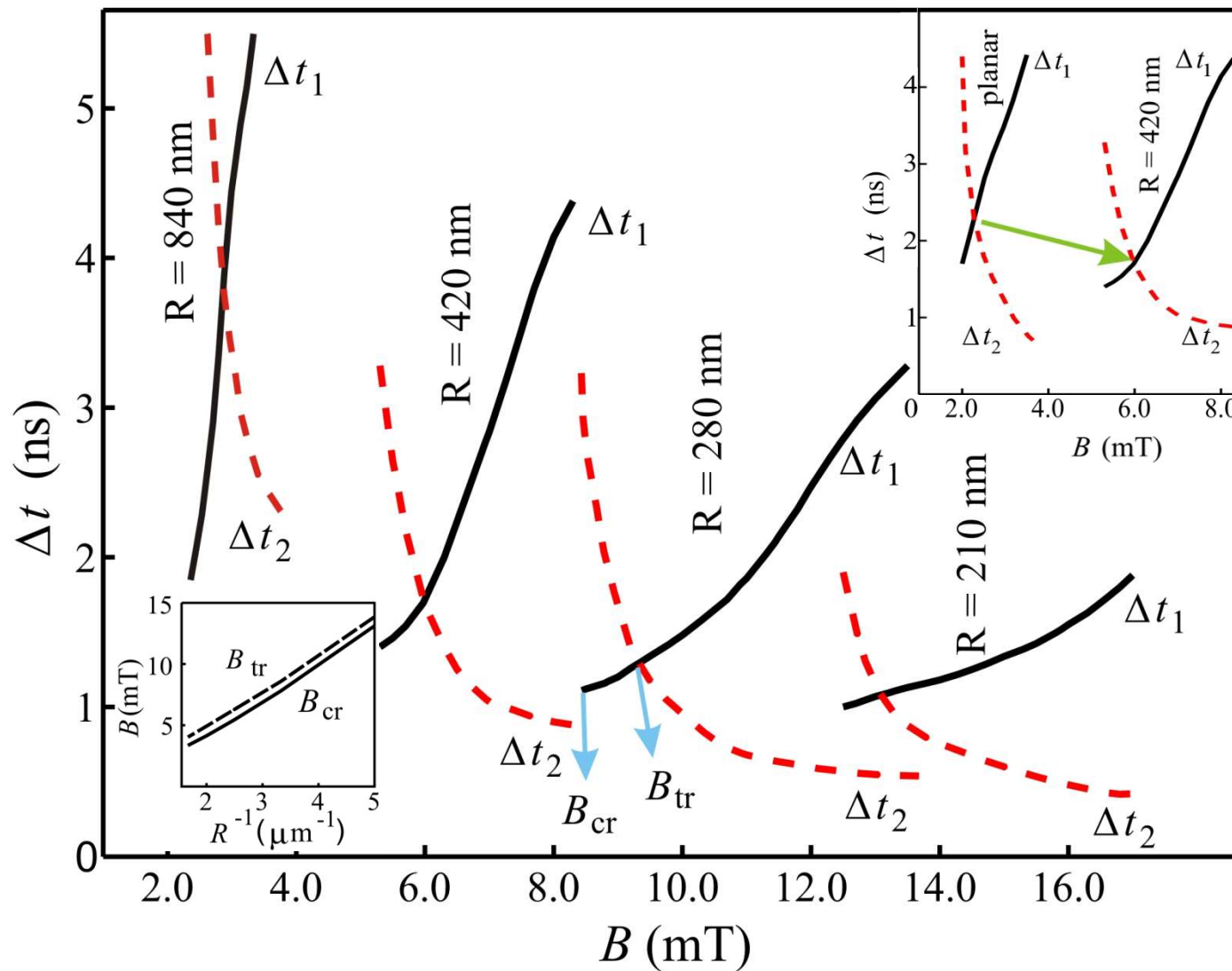
The multi-vortex regime for a Nb tube of radius $R = 500$ nm and length $L = 3.5$ μm with a slit of width $1/30 \times 2\pi R = 105$ nm at $\Phi/\Phi_0 = 22.5$.

$$\mathbf{F} = \mathbf{j}_{tot} \times \mathbf{B} \quad \mathbf{j}_{tot} = \mathbf{j} + \mathbf{j}_M + \mathbf{j}_{vortices}$$

Characteristic times of dynamics



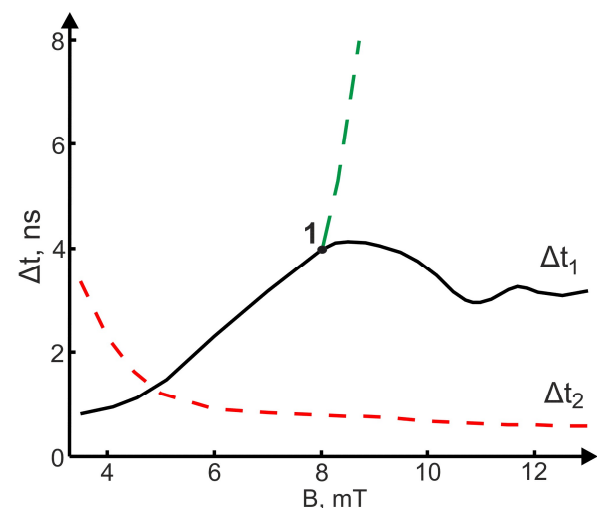
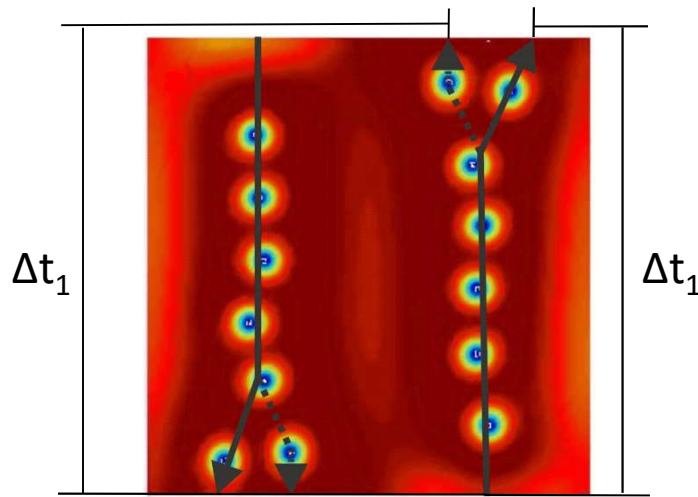
4. Effects of curvature



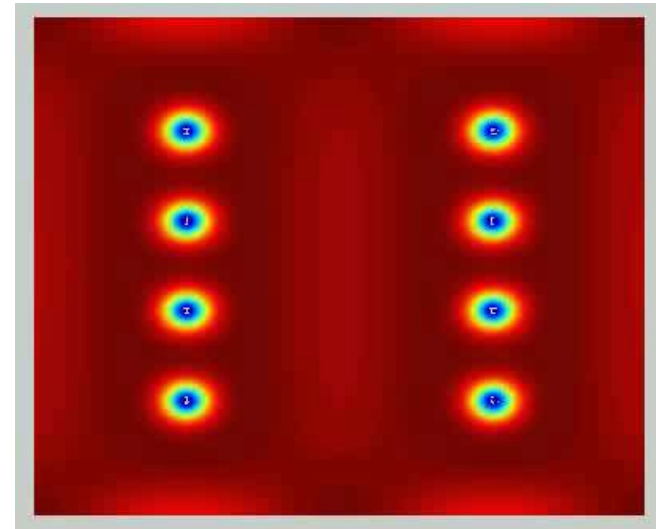
Control over the transition magnetic field by rolling up a film into a tube

7. Behavior of the vortex dynamics in the system with symmetrical electrodes

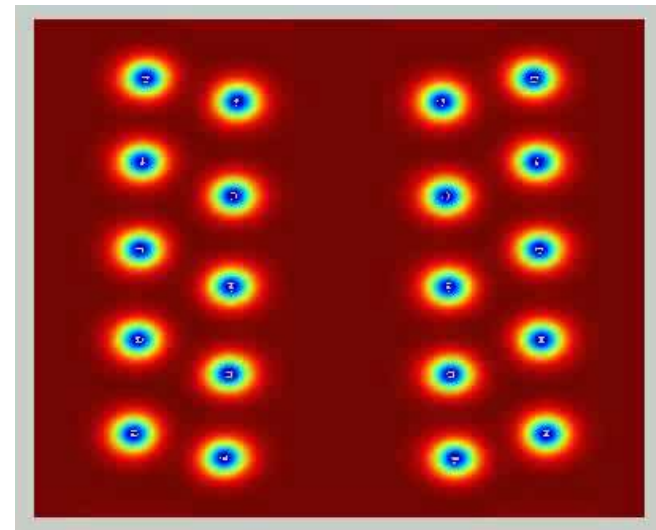
Snapshot at $B = 9$ mT and $\Delta t(B)$



$B = 7$ mT

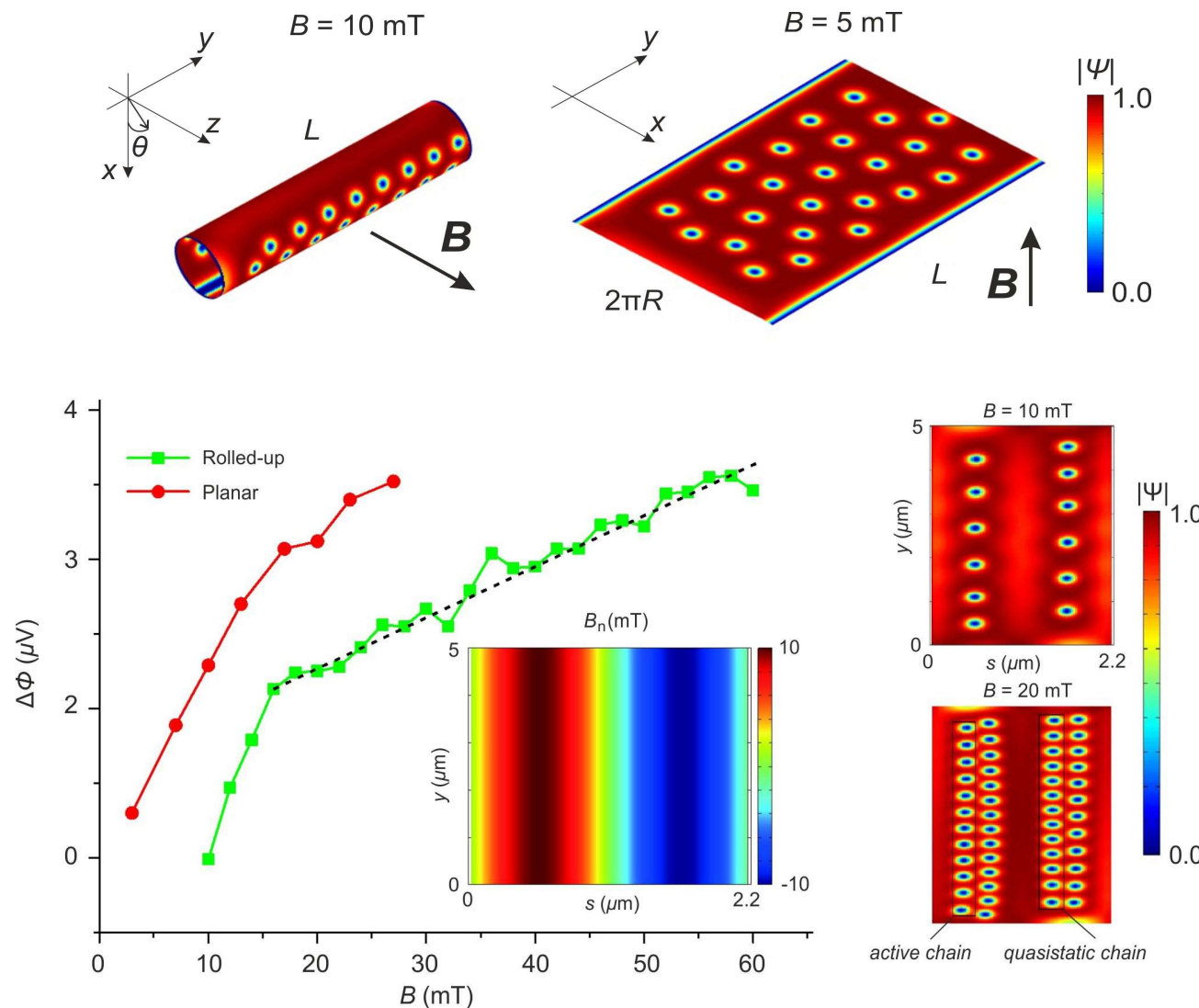


$B = 9$ mT

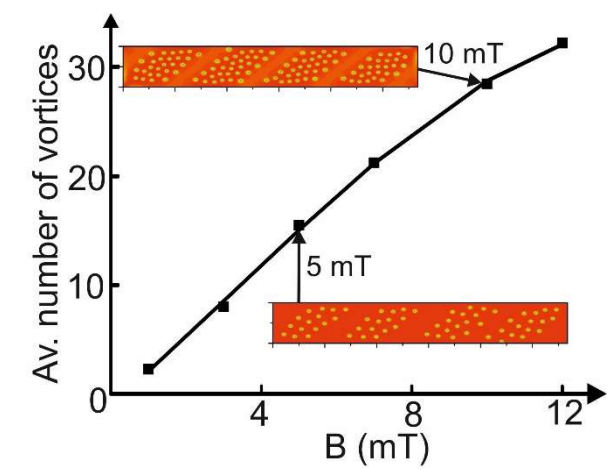
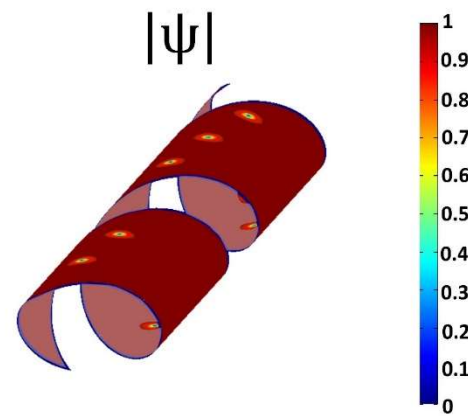
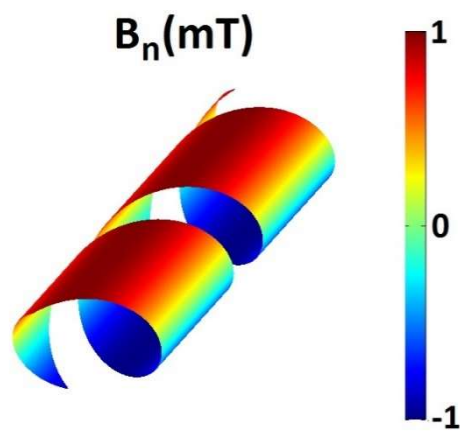
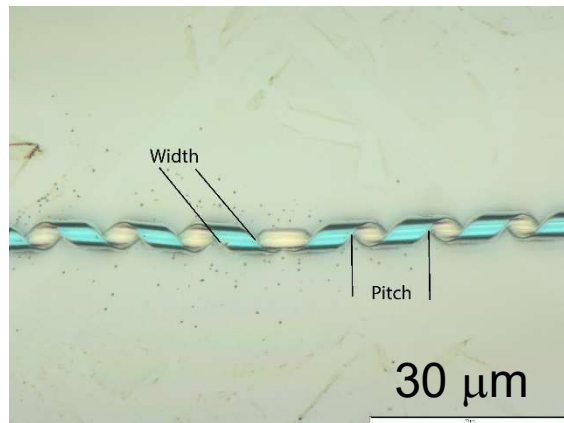


R. O. Rezaev, E. A. Levchenko, O. G. Schmidt
and V. M. Fomin, Rus. Phys. J. 58, 623 (2015)

Voltage induced by superconducting vortices in open nanostructured microtubes

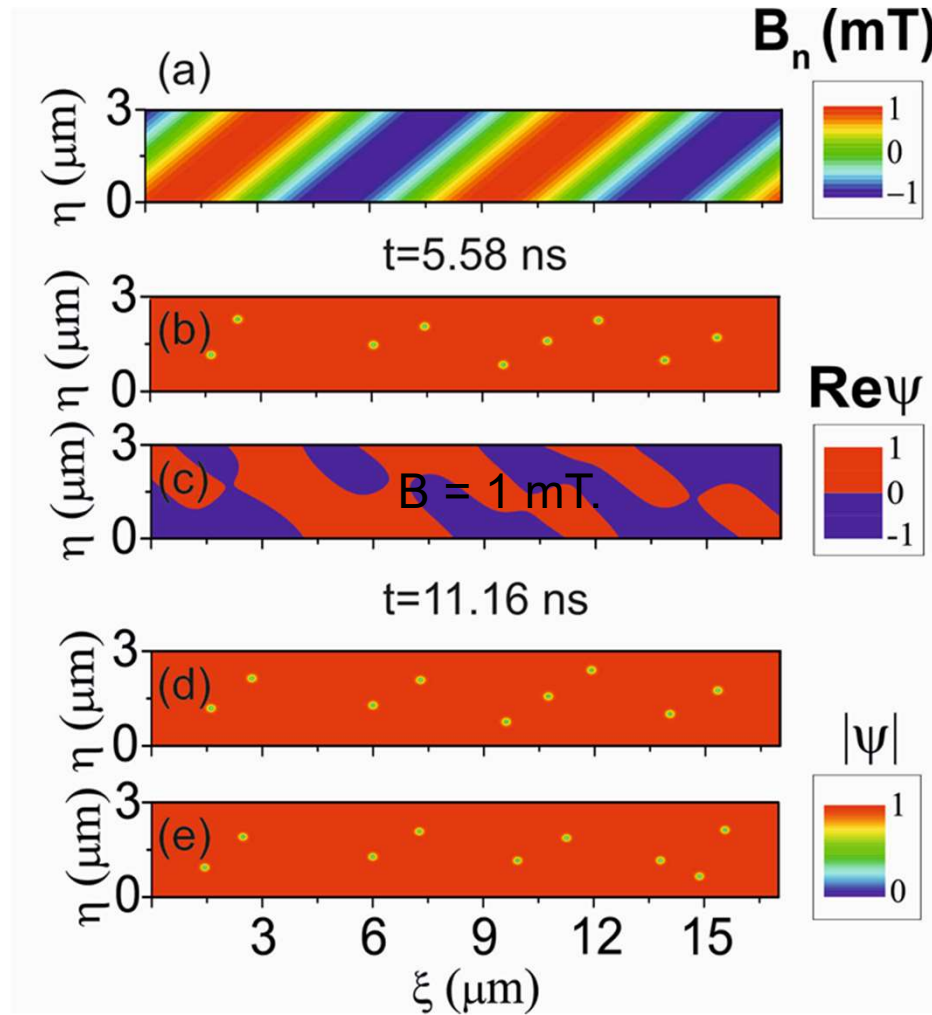


Superconductor helices



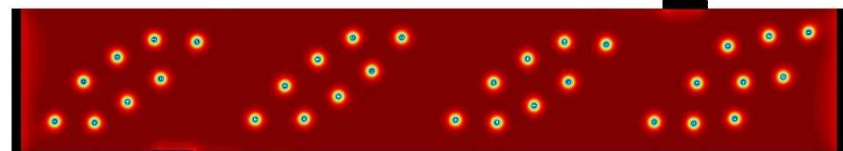
V. M. Fomin, R. O. Rezaev, E. A. Levchenko, D. Grimm, O. G. Schmidt,
J. of Physics Condensed Matter 29, 395301 (2017).

Incommensurability effect in microcoils



$R=0.96 \mu\text{m}$, $W=3 \mu\text{m}$, $P=6 \mu\text{m}$, $L=17.02 \mu\text{m}$, $B = 1 \text{ mT}$

Superconducting spirals: dynamics



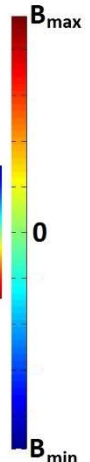
Outer half-turns

$$\Delta t_1 = 12.83 \pm 0.26 \text{ ns.}$$

$$\Delta t_2 = 5.09 \pm 0.23 \text{ ns.}$$



B_{norm}

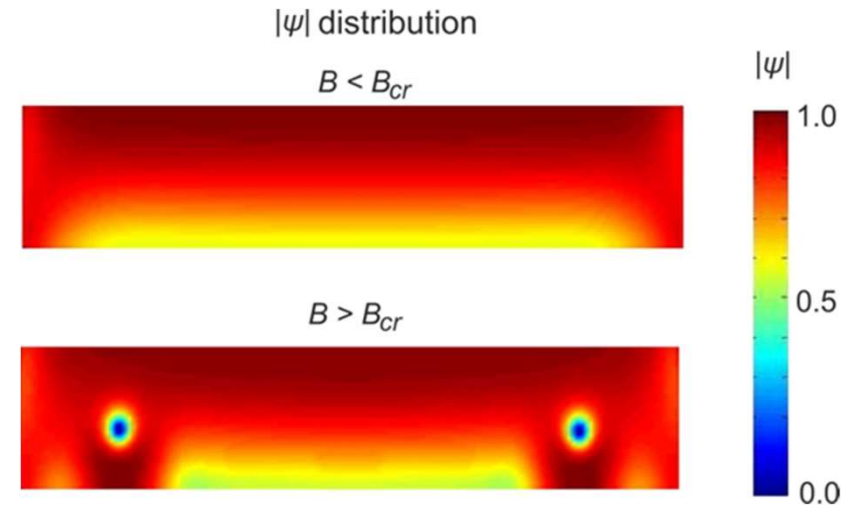
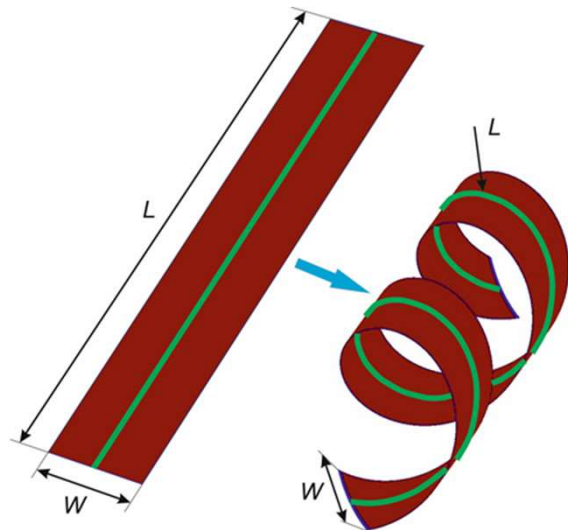


Inner half-turns

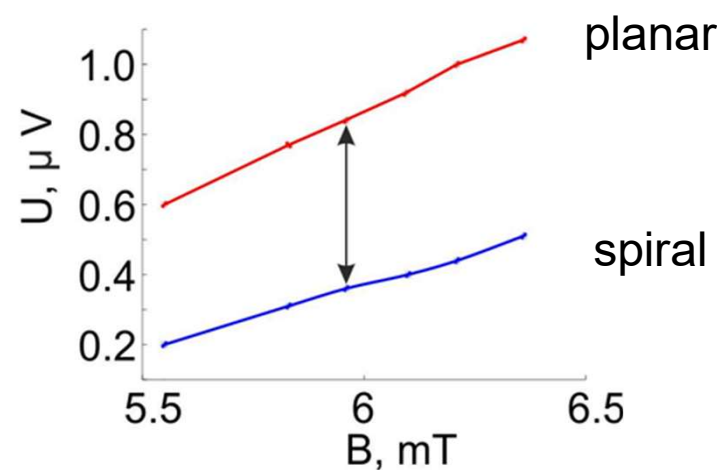
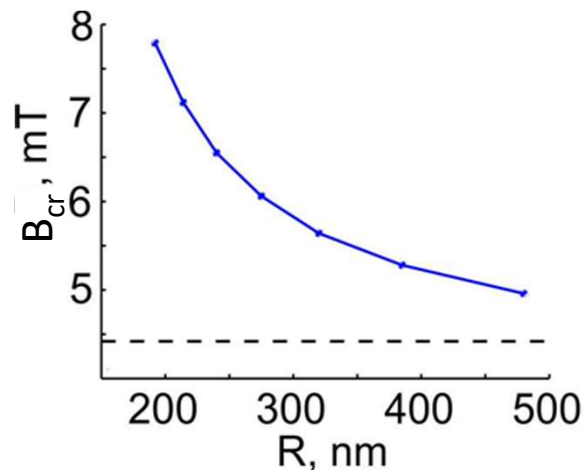
$$\Delta t_1 = 51.59 \pm 0.13 \text{ ns.}$$

$$\Delta t_2 = 17.66 \pm 0.37 \text{ ns.}$$

Superconducting spirals: critical magnetic field



$L = 6.5\mu\text{m}$, width $W = 1 \mu\text{m}$, $j = 2.0$, $B_{cr} = 4.42 \text{ mT}$



Conclusions

1. Topology-driven quantum interference effects in doubly connected nanoarchitectures is an important playground for the quantum mechanical paradigm.
2. Core-multishell GaAs/AlAs nanowires are shown to be an excellent platform for manifestations of the Aharonov–Bohm effect of neutral and charged excitons.
3. Rolled up nanoarchitectures are promising for thermoelectric applications owing to a possibility of reduction of the thermal conductivity without degradation of the electronic transport.
4. Interplay of a curved geometry with an inhomogeneous transport current in superconductor nanoarchitectures effectively controls topologically nontrivial order parameter distributions and vortex states.

Acknowledgements

- COST Action no. CA16218 “Nanoscale Coherent Hybrid Devices for Superconducting Quantum Technologies” (European Union)
- FO 956 /4-1 MULTISHELL German Research Foundation (DFG, Germany)
- FO 956 /5-1 SUPROLL German Research Foundation (DFG, Germany)
- Alexander von Humboldt Foundation (Germany)



Deutsche
Forschungsgemeinschaft



Alexander von Humboldt
Stiftung/Foundation

Thank you for your attention

